https://doi.org/10.5194/egusphere-2025-5430
Preprint. Discussion started: 21 January 2026

Ocean–atmosphere turbulent flux algorithms in Earth system models do not always converge to unique and physical solutions: analysis and potential remedy in E3SMv2

Justin Dong[1], Michael A. Brunke[2], Xubin Zeng[2], Carol S. Woodward[1], Hui Wan[3], and Christopher J. Vogl[1]

[1]Center for Applied Scientific Computing, Lawrence Livermore National Laboratory, Livermore, CA, USA
[2]Department of Hydrology and Atmospheric Sciences, University of Arizona, Tucson, AZ, USA
[3]Atmospheric, Climate, and Earth Sciences Division, Pacific Northwest National Laboratory, Richland, WA, USA

Correspondence: Justin Dong (dong9@llnl.gov)

Abstract.

The development of physics parameterizations in Earth system models typically emphasizes whether the intended physics is reasonably represented, while mathematical aspects such as solvability of the governing equations and convergence of the numerical algorithms used to approximate their solutions receive far less attention. In this paper, we examine these mathematical issues for a widely used ocean–atmosphere turbulent flux parameterization and its implementation in the Energy Exascale Earth System Model version 2 (E3SMv2). We show that, under simulated meteorological conditions, the parameterization can yield no solution or multiple (including unintended) solutions. These problems arise primarily from (1) a discontinuity in the formulation of the neutral exchange coefficients and (2) the use of an *ad hoc* limiter on the Monin–Obukhov length to address a singularity in its definition. Compounding these problems is the fact that interventions of calculations such as limiters are often thought to have only a "minor" effect on numerical algorithms and are not documented in technical model descriptions. To address these solvability issues, we propose (1) a regularization that enforces continuity in the neutral exchange coefficients and (2) an adaptive procedure for selecting limiting values of the Monin–Obukhov length based on mathematical analysis of solution uniqueness. Implementing these revisions in E3SMv2 leads to statistically significant changes in the simulated latent heat fluxes over the mid-latitude oceans in the winter hemisphere as well as over the subtropical and tropical oceans. Overall, this work improves the well-posedness and numerical accuracy of ocean–atmosphere turbulent flux calculations in E3SMv2. Moreover, because discontinuities and *ad hoc* limiters are frequently encountered in physics parameterizations, this work serves as an example of how non-existence and non-uniqueness issues in parameterizations can be identified, analyzed, and resolved.

1 Introduction

Turbulent fluxes at the Earth's surface are major contributors to the exchange of mass, heat, and momentum between the atmosphere and the other components of the Earth system. Accurate calculations of these fluxes are crucial for faithful simulations

https://doi.org/10.5194/egusphere-2025-5430
Preprint. Discussion started: 21 January 2026

of the responses and feedbacks related to component interactions. While the atmosphere interacts with various types of surfaces such as ocean, land, sea ice, and land ice, this study considers only the ocean–atmosphere interface.

Since ocean–atmosphere turbulent fluxes occur at spatial and temporal scales that are much smaller than the typical Earth System Model (ESM) grid spacing of a few tens to a few hundreds of kilometers, surface turbulent flux parameterizations, which rely on Monin-Obukhov Similarity Theory (MOST, Monin and Obukhov, 1954), are employed to relate these fluxes to the resolved quantities such as wind speed, temperature, and specific humidity in the lowest atmospheric layer, as well as sea surface temperature and humidity. Many different ocean–atmosphere turbulent flux parameterizations have been developed in the past several decades based on observational data from various oceanic regimes (see, e.g., Large and Pond, 1982, 1981; Zeng et al., 1998; Fairall et al., 2003). While the particular physical effects considered vary from parameterization to parameterization, e.g., some consider convective wind gustiness or reduction of surface humidity due to salinity of ocean water (Zeng et al., 1998; Brunke et al., 2002, 2003), each parameterization consists of a system of nonlinear equations whose solutions are approximated iteratively, for instance using a fixed-point iteration (Isaacson and Keller, 1994).

A number of studies have shown that ESMs are quite sensitive to the choice of ocean–atmosphere turbulent flux parameterization (see, e.g., Reeves Eyre et al., 2021; Harrop et al., 2018; Large and Caron, 2015), as, for instance, different parameterizations can produce a wide spread of turbulent fluxes in weak or strong wind conditions (Chang and Grossman, 1999; Zeng et al., 1998). While those studies have focused on the modeled physics, there has been no systematic analysis carried out to ascertain whether or not the aforementioned parameterizations are *well-posed* from a mathematical perspective — that is, whether or not the equation set used in a parameterization has a unique solution for each set of input values. In other words, underpinning much of the analysis in the literature of turbulent flux parameterizations is the assumption that the numerical methods used therefore converge to a unique solution, but the validity of this assumption and the potential impacts of its violation are largely overlooked. Such considerations are not merely academic but have significant impact on computed turbulent fluxes, as we demonstrate in this paper.

The focus of this study is on the well-posedness of the equations in a widely used ocean–atmosphere turbulent flux-parameterization based on the work of Large and Pond (1981) and Large and Pond (1982), hereafter referred to as the Large and Pond parameterization. This parameterization is currently the default in the Energy Exascale Earth System Model version 2 (E3SMv2, Golaz et al., 2022) and version 3 (E3SMv3, Xie et al., 2025), the Community Earth System Model (CESM, Hurrell et al., 2013; Danabasoglu et al., 2020), and several models based on CESM, such as the Taiwanese Earth System Model (TaiESM, Lee et al., 2020), the Norwegian Earth System Model version 1 (NorESM v1, Bentsen et al., 2013), the Euro-Mediterranean Center on Climate Change's ESM (CMCC-ESM2, Lovato et al., 2022), and the Regional Arctic System Model (RASM, Cassano et al., 2017). We demonstrate that under certain meteorological conditions, the equations of the parameterization have either no solution or multiple solutions, some of which correspond to physically-unrealistic values of the turbulent fluxes. The consequence is a computed turbulent flux with large errors which are then propagated back into the ocean and atmosphere models.

We focus on discontinuous neutral exchange coefficients and *ad hoc* limiters applied to the Obukhov length as key causal factors in the lack of well-posedness in the equations of the Large and Pond parameterization. Abrupt changes in physical

https://doi.org/10.5194/egusphere-2025-5430
Preprint. Discussion started: 21 January 2026

quantities sometimes have a physical basis. For instance, the neutral heat exchange coefficient from Large and Pond (1982) is derived from ship and deep stable water tower data that show a potential separation of values based on atmospheric stratification. In such cases, a discontinuity in the model formulation can be viewed a simple approximation of the abrupt changes. Limiters are commonly used in ESMs in a wide variety of contexts preventing physical quantities from taking negative values, for instance in the Cloud Layers Unified By Binormals (CLUBB) model of clouds and turbulence (see discussions in Zhang et al., 2023a). Discontinuous quantities might not be as prevalent but examples are not hard to find, for instance in cloud microphysics schemes (Morrison and Gettelman, 2008; Santos et al., 2020). And yet, the impact of these features on well-posedness and algorithm convergence is often overlooked. Indeed, limiters are often not documented in published literature and sometimes even excluded from technical model descriptions despite their potential to cause unwanted behavior in numerical algorithms. For example, E3SMv2's ocean–atmosphere turbulent flux algorithms are inherited from CESM, whose implementation utilizes the same Obukhov length limiters which are notably absent from the model's technical documentation (Neale et al., 2012). Only recently have ESM developers begun to address the lack of documentation of key model features such as limiters and noting that these seemingly "minor" interventions often have outsized effects on Earth system simulations (see, e.g., Kawai et al., 2022).

In this paper, we use the Large and Pond parameterization implemented in E3SMv2 as an example to demonstrate how mathematical issues of well-posedness manifest themselves in practice and how the potential causes can be diagnosed. Based on those analyses, we present two techniques to ensure that the turbulent flux parameterization is well-posed. These techniques include (1) simple polynomial interpolation to regularize discontinuous heat exchange coefficients to ensure solution existence and (2) an adaptive adjustment to Monin-Obukhov length limiters to ensure solution uniqueness. We demonstrate that the proposed techniques for addressing solution non-existence and non-uniqueness have statistically significant impacts on the computed turbulent fluxes. The techniques and analysis in this work provide a foundation for future efforts aimed at improving the accuracy and efficiency of turbulent flux algorithms at other interfaces (e.g. sea ice, land). More generally, given the fact that limiters are widely used in ESMs and discontinuities in parameterizations are not uncommon, the work presented here may provide inspirations for assessing and addressing potential issues of well-posedness in other ESMs and in parameterizations of other subgrid-scale processes.

The rest of the paper is organized as follows. In Sect. 2, we provide an overview of the ocean–atmosphere surface flux parameterization and its numerical implementation in E3SMv2. In Sects. 3 and 4, we analyze issues of well-posedness and present modifications to ensure well-posedness. Sect. 5 presents the sensitivity of E3SMv2 simulations to the proposed modifications, followed by conclusions in Sect. 6.

2 Model description and analysis overview

In this section, we describe the Large and Pond ocean–atmosphere turbulent flux parameterization (Large and Pond, 1981, 1982) and the numerical methods used to compute the turbulent fluxes in E3SMv2. While this description is focused on methods used in E3SM, it is also valid for the other models which utilize this parameterization.

https://doi.org/10.5194/egusphere-2025-5430
Preprint. Discussion started: 21 January 2026

2.1 Terminology

The following terminology shall be used frequently hereafter. Of particular note is that we make a distinction between the turbulent flux *parameterization* and the turbulent flux *algorithm*.

- *Turbulent flux parameterization*: the equations that describe the scaling parameters, u_*, θ_*, and q_*, i.e. Eq. (13) in Sect. 2.3.
- *Turbulent flux algorithm or iterative method*: the numerical method used to compute a solution of the turbulent flux parameterization, e.g. Alg. 1 in Sect. 2.3. Such an algorithm/method is called *convergent* if the iterates converge to a solution of the parameterization.
- *Equations underlying the turbulent flux algorithm*: the turbulent flux parameterization.
- *Existence of a solution (to the underlying equations)*: at least one solution can be determined which satisfies the equations underlying the turbulent flux algorithm.
- *Uniqueness of a solution (to the underlying equations)*: exactly one solution satisfies the equations underlying the turbulent flux algorithm.
- *Well-posed equation or parameterization*: an equation or system of equations for which there exists a unique solution.

2.2 E3SMv2

E3SMv2 is an ESM developed by the U.S. Department of Energy (Golaz et al., 2022) that includes components for the atmosphere, land, ocean, sea ice, land ice, rivers, and human systems. In this study, we use the atmosphere component, EAMv2, in the "uncoupled" mode, i.e., with interactive land and river components, while external forcing conditions including sea surface temperatures and sea ice fraction, aerosol emissions, etc. are specified using the climatological mean of 2005–2014 with repeating annual cycles. We refer to such simulations as F2010 following E3SM's naming convention for model configurations. Overviews and some more detailed descriptions of EAMv2 can be found in Golaz et al. (2022), Ma et al. (2022), Rasch et al. (2019), and Xie et al. (2018).

2.3 Parameterization of ocean–atmosphere turbulent fluxes

The turbulent fluxes of interest in this work are the surface wind stress (τ) in $\mathrm{N\,m^{-2}}$, sensible heat flux (SH) in $\mathrm{W\,m^{-2}}$, and latent heat flux (LH) in $\mathrm{W\,m^{-2}}$ defined as (see, e.g., Eqs. 1-3 in Brunke et al., 2003)

$$\tau = \rho_a \left[\left(\overline{w'u'}\right)^2 + \left(\overline{w'v'}\right)^2 \right]^{\frac{1}{2}}, \tag{1}$$

$$\mathrm{SH} = \rho_a C_p \overline{w'\theta'}, \tag{2}$$

$$\mathrm{LH} = \rho_a L_v \overline{w'q'}, \tag{3}$$

https://doi.org/10.5194/egusphere-2025-5430
Preprint. Discussion started: 21 January 2026

where the notation $\overline{w'\Phi'}$ denotes the (eddy) covariance between the vertical velocity w (in m s^{-2}) and another quantity Φ. Here, u, v, q, and θ are the zonal and meridional components of horizontal wind in m s^{-1}, specific humidity in kg kg^{-1}, and potential temperature in K, respectively; C_p is the specific heat of moist air at constant pressure in J kg^{-1} K^{-1}; and L_v is the latent heat of vaporization in J kg^{-1}.

Numerical models require turbulent flux parameterizations in which the eddy covariances are often expressed in terms of resolved (bulk) meteorological quantities, in the form of

$$\left[\left(\overline{w'u'}\right)^2 + \left(\overline{w'v'}\right)^2\right]^{\frac{1}{2}} = \quad C_{\mathrm{D}} S U\,, \tag{4}$$

$$\overline{w'\theta'} = -C_{\mathrm{H}} S \Delta\theta\,, \tag{5}$$

$$\overline{w'q'} = -C_{\mathrm{E}} S \Delta q\,, \tag{6}$$

where U is wind speed in $\mathrm{m\,s^{-1}}$; S is the wind speed in $\mathrm{m\,s^{-1}}$ including wind gustiness if the latter is considered, and $S = U$ if gustiness is not considered; $\Delta\theta = \theta_a - \theta_s$ is the potential temperature difference between the respective values in the atmosphere (θ_a) and at the surface (θ_s), in K; $\Delta q = q_a - q_s$ is the specific humidity difference between the respective values in the atmosphere (q_a) and at the surface (q_s), with a unit of kg water vapor per kg air. The central goal in the development of a parameterization is to provide formulae for C_{D}, C_{H}, and C_{E}, the dimensionless turbulent exchange coefficients for momentum, heat, and moisture, respectively.

A practical complication is that these exchange coefficients are typically formulated as piecewise empirical fits of observational data dependent on stability of the surface layer, while this stability depends, in turn, on the surface fluxes that we are trying to parameterize. This results in a situation where a set of nonlinear equations needs to be solved to determine both the stability and the exchange coefficients. More specifically, the stability of the surface layer is typically described using the dimensionless Obukhov stability parameter ζ defined as

$$\zeta(u_*, \theta_*, q_*) = z/L(u_*, \theta_*, q_*), \tag{7}$$

where z is height above the surface and L is Monin-Obukhov length. u_*, θ_* and q_* are the scaling parameters for momentum, heat and moisture, respectively, from Monin-Obukhov similarity theory (see, e.g., Brunke et al., 2003, Eq. 4-6), namely

$$u_*^2 = \left[\left(\overline{w'u'}\right)^2 + \left(\overline{w'v'}\right)^2\right]^{\frac{1}{2}}, \tag{8}$$

$$\theta_* = -\frac{\overline{w'\theta'}}{u_*}, \tag{9}$$

$$q_* = -\frac{\overline{w'q'}}{u_*}. \tag{10}$$

An expression for L can be found in Eq. (4) of Zeng et al. (1998), namely,

$$L(u_*, \theta_*, q_*) = \frac{u_*^2 \theta_v}{\kappa g \theta_{v*}} = \frac{u_*^2 \theta_a (1 + 0.61 q_a)}{\kappa g \left[\theta_* (1 + 0.61 q_a) 0.61 \theta_a q_*\right]}. \tag{11}$$

https://doi.org/10.5194/egusphere-2025-5430
Preprint. Discussion started: 21 January 2026

The symbols κ and g denote the dimensionless von Kármán constant of $\sim$0.4 and gravitational acceleration of $\sim$9.8 $\mathrm{m}\cdot\mathrm{s}^{-2}$, respectively. The sign of ζ dictates the stability of the surface layer, with $\zeta < 0$ corresponding to unstable, $\zeta = 0$ to neutral, and $\zeta > 0$ to stable conditions.

The Large and Pond parameterization used in E3SMv2 and various other models expresses the exchange coefficients C_{D}, C_{H}, and C_{E} using the so-called neutral exchange coefficients C_{DN}, C_{HN}, and C_{EN}, a neutral 10-m wind speed $u_{10\mathrm{N}}$, and functions of ζ. The detailed formulation can be found in Appendix A1, from which we can see that C_{D}, C_{H}, and C_{E} depend *directly* on $u_{10\mathrm{N}}$ and ζ, which are unknown, and on z. Furthermore, these exchange coefficients also have *indirect* dependencies on the known bulk meteorological variables since the stability parameter ζ depends on both the unknown u_*, θ_*, and q_* as well as known meteorological variables θ_a, q_a, etc. (see Eqs. (7) and (11)). To facilitate discussions and analyses later in the paper, we symbolically note these dependencies by

$$C_{(\mathrm{D,H,E})} = C_{(\mathrm{D,H,E})}\Big(u_{10\mathrm{N}}, \zeta(u_*, \theta_*, q_*); \boldsymbol{\xi}\Big)\,, \tag{12}$$

where, for ease of notation, we denote the aggregation of bulk meteorological variables by $\boldsymbol{\xi} = (U, \theta_a, \theta_s, z, \rho_a, q_a, q_s)^T$, with ρ_a being the density of air in $\mathrm{kg\,m}^{-3}$.

As elaborated in Appendix A2, one can define an additional set of coefficients $\widehat{C}_{(\mathrm{D,H,E})}$ by adjusting $C_{(\mathrm{D,H,E})}$ (see Eq. A11) to the height and stability of the atmospheric state variables. The set of equations used in E3SMv2 is based on these adjusted coefficients and is given by

$$\begin{cases} u_{10\mathrm{N}} = \dfrac{\widehat{C}_{\mathrm{D}}\Big(u_{10\mathrm{N}}, \zeta(u_*, \theta_*, q_*); \boldsymbol{\xi}\Big)}{\sqrt{C_{\mathrm{DN}}(u_{10\mathrm{N}})}} \cdot U\,, \\ u_* = \widehat{C}_{\mathrm{D}}\Big(u_{10\mathrm{N}}, \zeta(u_*, \theta_*, q_*); \boldsymbol{\xi}\Big) \cdot U\,, \\ \theta_* = \widehat{C}_{\mathrm{H}}\Big(u_{10\mathrm{N}}, \zeta(u_*, \theta_*, q_*); \boldsymbol{\xi}\Big) \cdot \Delta\theta\,, \\ q_* = \widehat{C}_{\mathrm{E}}\Big(u_{10\mathrm{N}}, \zeta(u_*, \theta_*, q_*); \boldsymbol{\xi}\Big) \cdot \Delta q\,. \end{cases} \tag{13}$$

Detailed expressions of $\widehat{C}_{\mathrm{D}}$, $\widehat{C}_{\mathrm{H}}$, and $\widehat{C}_{\mathrm{E}}$ can be found in Eq. (A13). A key feature relevant for this paper is that the expression for $\widehat{C}_{\mathrm{H}}$ involves an adjustment of the aforementioned neutral heat exchange coefficient, denoted by $\widehat{C}_{\mathrm{HN}}$, which is discontinuous by construction:

$$\widehat{C}_{\mathrm{HN}}\Big(\zeta(u_*, \theta_*, q_*)\Big) = \begin{cases} 0.0327, & \text{if } \zeta < 0 \\ 0.018, & \text{if } \zeta \geqslant 0. \end{cases} \tag{14}$$

The discontinuous construction of $\widehat{C}_{\mathrm{HN}}$ is based upon measurements from deep stable water towers and weather ships (Large and Pond, 1982) which show that the average measurements differ significantly for stable and unstable conditions, as explained by the text around Eq. (23) in Large and Pond (1982).

https://doi.org/10.5194/egusphere-2025-5430
Preprint. Discussion started: 21 January 2026

2.4 Numerical algorithm for solving the scaling parameter equations

Eq. (13) can be written more succinctly as

$$\boldsymbol{x} = \boldsymbol{f}\left(\boldsymbol{x};\boldsymbol{\xi}\right), \tag{15}$$

where $\boldsymbol{x} = (u_{10\mathrm{N}}, u_*, \theta_*, q_*)^T$, and $\boldsymbol{f}$ is the vector-valued function on the right-hand side of Eq. (13). In mathematics, solutions to Eq. (15) are referred to as *fixed points*. Since an analytic solution to Eq. (13) is not available, the scaling parameters and neutral 10-m wind speed must be approximated using an iterative method. A standard fixed-point iteration approximates the solution of the equation $\boldsymbol{x} = \boldsymbol{f}(\boldsymbol{x};\boldsymbol{\xi})$ by producing iterates of the form

$$\boldsymbol{x}_{n+1} = (1-\alpha)\boldsymbol{x}_n + \alpha\boldsymbol{f}(\boldsymbol{x}_n;\boldsymbol{\xi}), \tag{16}$$

where $0 < \alpha \leqslant 1$ is a damping parameter. Other (more advanced) solution algorithms are also available, as mentioned later in Sect. 3.6. In E3SMv2, a sequence of fixed-point iterations in the form of Eq. (16) with $\alpha = 1$ are utilized to update the neutral 10-m wind speed first followed by the scaling parameters, with the initial iterate $\boldsymbol{x}_0$ being derived from neutral stability conditions. The iterative method is summarized in Alg. 1. The specific sequential approach employed by E3SMv2 more generally falls under the umbrella of nonlinear Gauss-Seidel methods; we direct the interested reader to Ortega and Rockoff (1966) for a rigorous analysis of such methods.

Additionally, the E3SMv2 code applies an upper bound (limiter) to the Obukhov stability parameter in Eq. (13) to prevent its magnitude from growing too large throughout the course of the iterations. The limited stability parameter, which we denote by $\tilde{\zeta}$, is defined by

$$\tilde{\zeta}\Big(u_*, \theta_*, q_*; \zeta_{\max}\Big) = \min\Big(\big|\zeta(u_*, \theta_*, q_*)\big|, \zeta_{\max}\Big) \cdot \mathrm{sgn}\Big(\zeta(u_*, \theta_*, q_*)\Big). \tag{17}$$

We refer to the parameter $\zeta_{\max} > 0$ as the *limiting parameter*. Its value is set to 10 in E3SMv2 and ζ is replaced with $\tilde{\zeta}$ in Eq. (13). A detailed analysis of the stability limiter and its relationship with uniqueness of solutions of Eq. (13) is provided in Sect. 4.2.

Finally, it is worth noting that E3SMv2's default iterative algorithm uses a hardwired total of two iterations without checks on numerical convergence. Further discussions on this can be found in Sect. 3.5.

2.5 Offline analyses and E3SM simulations

The convergence of numerical methods used for finding fixed points requires at minimum that there exists at least one solution to the underlying equation Eq. (15). A system with no solutions can result in numerical methods oscillating between two values and never converging. If the system has multiple solutions, numerical methods may converge to an undesired (e.g. non-physical) solution. Thus, it is important that well-posedness of turbulent flux parameterizations be analyzed prior to the application of any numerical methods. To the best of our knowledge, this analysis has not yet been carried out for the Large and Pond parameterization or any other ocean–atmosphere turbulent flux parameterizations.

https://doi.org/10.5194/egusphere-2025-5430
Preprint. Discussion started: 21 January 2026

Algorithm 1 Default atmosphere-ocean iteration in E3SMv2.

Input: Bulk variables $\boldsymbol{\xi} = (U, \theta_a, \theta_s, z, \rho_a, q_a, q_s)^T$ and limiting parameter $\zeta_{\max}$.

Output: Approximation $(u_*)_n$, $(u_{10N})_n$, $(\theta_*)_n$, and $(q_*)_n$ to the turbulent flux parameterization Eq. (13).

function DEFAULTITERATION($\boldsymbol{\xi}$, $\zeta_{\max}$)

Compute the initial estimate based on neutral conditions:

$$
\begin{aligned}
(u_{10N})_0 &= U\,,\\
(u_*)_0 &= \sqrt{C_{DN}(U)}\cdot U\,,\\
(\theta_*)_0 &= \widehat{C}_{HN}(\Delta\theta)\cdot\Delta\theta\,,\\
(q_*)_0 &= \widehat{C}_{EN}\cdot\Delta q.
\end{aligned}
$$

Compute limited stability parameter $\tilde{\zeta}_0 = \tilde{\zeta}\Big((u_*)_0, (\theta_*)_0, (q_*)_0; \zeta_{\max}\Big)$ according to Eq. (17).

for $n = 1, 2$ **do**

Update 10-m neutral wind speed:

$$
(u_{10N})_n = \frac{\widehat{C}_D\Big((u_{10N})_{n-1}, \tilde{\zeta}_{n-1}; \boldsymbol{\xi}\Big)}{\sqrt{C_{DN}\Big((u_{10N})_{n-1}\Big)}}\cdot U.
$$

Apply updated 10-m neutral wind speed to simultaneously update scaling parameters:

$$
\begin{pmatrix} (u_*)_n \\ (\theta_*)_n \\ (q_*)_n \end{pmatrix} = \begin{pmatrix} \widehat{C}_D\Big((u_{10N})_n, \tilde{\zeta}_{n-1}; \boldsymbol{\xi}\Big)\cdot U \\ \widehat{C}_H\Big((u_{10N})_n, \tilde{\zeta}_{n-1}; \boldsymbol{\xi}\Big)\cdot\Delta\theta \\ \widehat{C}_E\Big((u_{10N})_{n-1}, \tilde{\zeta}_{n-1}; \boldsymbol{\xi}\Big)\cdot\Delta q \end{pmatrix}.
$$

Update stability parameter $\tilde{\zeta}_n = \tilde{\zeta}\Big((u_*)_n, (\theta_*)_n, (q_*)_n; \zeta_{\max}\Big)$.

end for

return $(u_*)_n, (\theta_*)_n, (q_*)_n$.

Our well-posedness analysis presented here consists of two components. The first part, described in Sect. 3, sheds lights on whether there always exists a solution to Eq. (13). The second part, described in Sect. 4, answers the question of whether a solution to Eq. (13) is always unique. The analysis uses theoretical reasoning as well as offline calculations based on output from E3SMv2. The E3SMv2 data used therein were obtained from a 10-year F2010 simulation performed at EAMv2's standard grid spacing of about 165 km for the atmospheric physics parameterization (Hannah et al., 2021). The simulation uses E3SMv2's default ocean–atmosphere flux algorithm detailed in Alg. 1 and hence is referred to as the CTRL simulation hereafter. Daily instantaneous values of the atmospheric and oceanic conditions used by the flux calculations were captured and archived using the online diagnostics tool CondiDiag from Wan et al. (2022). These values were then used to identify grid cells in which the

https://doi.org/10.5194/egusphere-2025-5430
Preprint. Discussion started: 21 January 2026

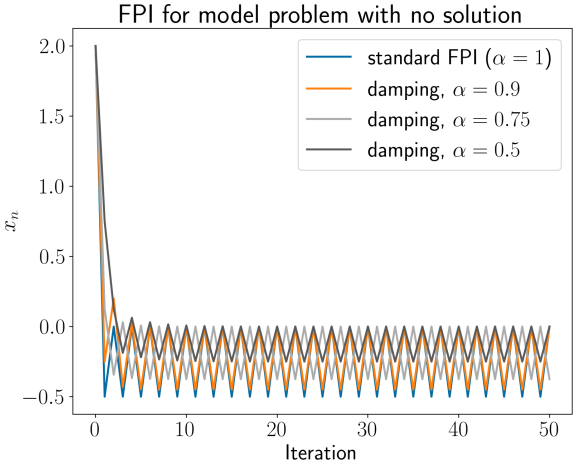

Figure 1. Results of fixed-point iteration applied to a simple, illustrative example with no actual solution due to discontinuity (see Sect. 3.1 and Eq. (18)). Shown here is the iterate x_n against the number of iterations. The various lines correspond to different values of the damping parameter α.

iterative method in Alg. 1 (a) is not able to converge to any solution or (b) converges to more than one solution depending on the initial guess.

Based on the results of the well-posedness analysis, revisions to the default flux algorithm are proposed in Sects. 3 and 4. Key features of the proposed revisions are analyzed in these sections using offline calculations. After that, Sect. 5 presents a 10-year simulation SENS, with the proposed revisions included, to assess the impact on the simulated long-term climatology, with a focus on the parameterized surface fluxes.

3 Analyzing and addressing existence issues

One approach to analyzing existence of solutions to Eq. (13) is to consider the system in the form $\boldsymbol{x} = \boldsymbol{f}(\boldsymbol{x};\boldsymbol{\xi})$. Solutions to this system lie on the surface described by the intersections of the two graphs $\boldsymbol{x}$ and $\boldsymbol{f}(\boldsymbol{x};\boldsymbol{\xi})$. If $\boldsymbol{f}(\boldsymbol{x};\boldsymbol{\xi})$ contains any discontinuities, then $\boldsymbol{x}$ and $\boldsymbol{f}(\boldsymbol{x};\boldsymbol{\xi})$ may not intersect, and hence Eq. (13) may not have a solution. From this perspective, one should examine any potential discontinuities in $\boldsymbol{f}$. For completeness, we note that solutions to $\boldsymbol{x} = \boldsymbol{f}(\boldsymbol{x};\boldsymbol{\xi})$ may still exist despite discontinuities in $\boldsymbol{f}(\boldsymbol{x};\boldsymbol{\xi})$, an abstract example of which is shown in Appendix B. Therefore, our analysis begins with identifying discontinuities, followed by investigating whether the discontinuities cause non-existence of a solution or non-convergence of a numerical algorithm. Below, we first show a simple, illustrative example and then apply this analysis strategy to the Large and Pond parameterization implemented in E3SMv2.

https://doi.org/10.5194/egusphere-2025-5430
Preprint. Discussion started: 21 January 2026

3.1 A simple illustrative example

To demonstrate how iterative methods may behave in the presence of a discontinuity in $\boldsymbol{f}(\boldsymbol{x};\boldsymbol{\xi})$, we first consider a minimal model problem which still captures the key issue. Suppose we are interested in solutions to $x = f(x)$, where $f(x)$ is defined by

$$f(x) = \begin{cases} x + 1/2, & x \leqslant 0 \\ -1/2, & x > 0. \end{cases} \tag{18}$$

One can easily verify by hand or graphically that this equation has no solutions. We apply the fixed-point iteration described by Eq. (16) with 100 iterations to this equation. While our goal is to show the behavior of this iteration for this example using the same settings as those in E3SMv2 (i.e. no damping, $\alpha = 1$), we also provide results with damping (i.e. $0 < \alpha < 1$), which can be viewed as reducing the "step size" of the iterates. The results in Fig. 1 demonstrate that x_n oscillates infinitely between two values for each of the damping parameters used.

The magnitude of the oscillation depends on the value of the damping parameter as well as particular features of the function $f(x)$ at the discontinuity. By using a very small damping parameter, one can reduce the size of the oscillations in the iterations, but it is important to note that the approximate solution will not satisfy the equation $x = f(x)$ because the equation has no actual solution.

3.2 Discontinuities and oscillations in E3SMv2

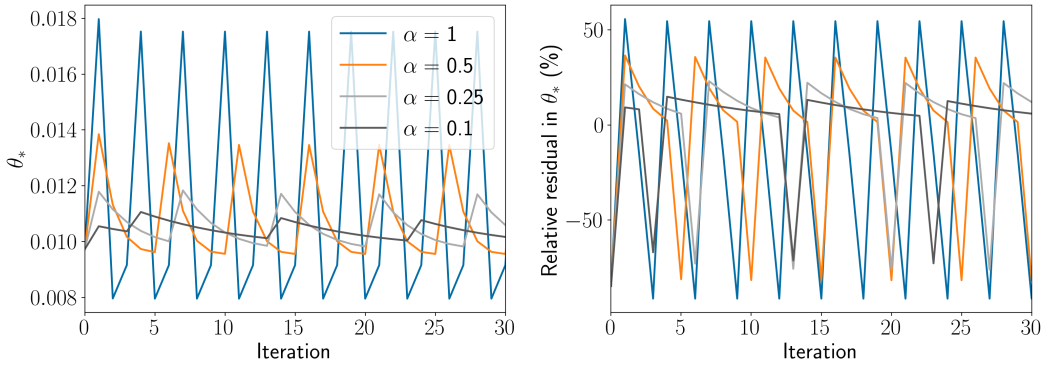

Figure 2. The iterate $(\theta_*)_n$ and its relative residual $|\boldsymbol{f}_3\left((u_*)_n, (u_{10\mathrm{N}})_n, (\theta_*)_n, (q_*)_n\right) - (\theta_*)_n|/|(\theta_*)_n + \epsilon_3|$ when approximating the solution of the turbulent flux parameterization in Eq. (13) with conditions described by Eq. (20). The iterates are described by Alg. 1 with the exception that 100 iterations are performed rather than 2 and damping is employed. For visual clarity, only the first 30 iterations are shown here.

We next turn our attention to the equations and algorithm in E3SMv2. As documented in Sect. 2.3, the adjusted neutral heat exchange coefficient $\widehat{C}_{\mathrm{HN}}$ is defined in a piecewise constant manner for stable and unstable conditions (see Eq. (14)). As a result, the right-hand side of the third equation in Eq .13, hereafter denoted by $\boldsymbol{f}_3$ for brevity, has a discontinuity at $\zeta = 0$ (neutral stability).

https://doi.org/10.5194/egusphere-2025-5430
Preprint. Discussion started: 21 January 2026

Using 10 years of model output from the E3SMv2 CTRL simulation described in Sect. 2.5, we apply the default iterative method in Alg. 1 while replacing the fixed number of iterations with a variable number of iterations and a stopping criterion based on the relative residual

$$\mathcal{R}(\boldsymbol{x};\boldsymbol{\xi}) := \sqrt{\sum_{i=1}^{4}\left|\frac{\boldsymbol{x}_i - \boldsymbol{f}_i(\boldsymbol{x};\boldsymbol{\xi})}{\boldsymbol{x}_i + \epsilon_i}\right|^2}. \tag{19}$$

The addition of the constant ϵ_i in the denominator of Eq. (19) is designed to ensure that the residual is well-defined even when $\boldsymbol{x}_i$ is small. The stopping criterion used in the offline analysis was $\mathcal{R}(\boldsymbol{x};\boldsymbol{\xi}) < 10^{-10}$ with $\epsilon_1 = 10^{-3}$, $\epsilon_2 = 10^{-3}$, $\epsilon_3 = 10^{-5}$, $\epsilon_4 = 10^{-8}$ for $u_{10\mathrm{N}}$, u_*, θ_*, and q_*, respectively. We filter the E3SMv2 data to identify conditions for which this stopping criterion could not be satisfied after a maximum of 1000 iterations.

One example of problematic neutral-stability conditions that we identified from E3SMv2 output is the following combination:

$$\begin{cases} U = 0.35 \text{ m/s}, \quad z = 13.36 \text{ m}, \quad \theta_s = 299.29 \text{ K}, \\ \theta_a = 299.83 \text{ K}, \quad q_a = 18.85 \text{ g/kg}. \end{cases} \tag{20}$$

We apply to this example E3SMv2's default numerical algorithm documented in Alg. 1 except with the fixed 2 iterations replaced by 100 iterations and show results for the iterate $(\theta_*)_n$ in the left panel of Fig. 2, where the oscillatory feature is clear. If Eq. (13) were well-posed and the fixed-point iteration were convergent, we could define a relative residual in the form of $|\boldsymbol{f}_3((u_*)_n, (\theta_*)_n, (q_*)_n) - (\theta_*)_n|/|(\theta_*)_n + \epsilon_3|$, and we would expect this residual to decrease, eventually to very small values close to machine epsilon, as the iteration proceeds. For the conditions described by Eq. (20), however, the relative residual resulting from E3SM's default algorithm oscillates between about $+50\%$ to -110%, with the iterate $(\theta_*)_n$ jumping between two significantly different values, neither of which satisfies the equation $\theta_* = \boldsymbol{f}_3(u_*, u_{10N}, \theta_*, q_*)$. Moreover, while damping reduces the magnitude of the oscillations, it does not substantially reduce the magnitude of the relative residual, which still takes values as large as -70%.

It is worth noting that while we have observed oscillations in all solution variables, i.e., u_*, θ_*, q_*, and $u_{10\mathrm{N}}$, the oscillation in θ_* is the strongest. This observation, together with the known discontinuity in $\boldsymbol{f}_3$ as well as the resemblance between the oscillations in E3SMv2 and those in the simple problem discussed in Sect. 3.1, suggests that the oscillations in E3SMv2 may be caused by non-existence of the solution at $\zeta = 0$. While we are unable to rigorously prove that the turbulent flux parameterization in Eq. (13) has no solution for the conditions described by Eq. (20), we shall demonstrate in the remainder of this section that a modification to $\widehat{C}_{\mathrm{HN}}$ to remove the discontinuity at $\zeta = 0$ eliminates the oscillations entirely and allows the iteration to converge to a solution.

To further characterize the Earth system states associated with oscillations in the ocean–atmosphere flux parameterization, we perform offline calculations using 10 years of daily instantaneous output from E3SMv2 as mentioned in Sect. 2.5. In these offline calculations, we again apply Algorithm 1 until either the stopping criterion $\mathcal{R}(\boldsymbol{x}_n;\boldsymbol{\xi}) < 10^{-10}$ is reached or a maximum of 1000 iterations have been taken. Each data point is classified as either (i) exhibiting oscillatory behavior or (ii) having converged if the stopping criterion is reached. Since the focus here is on cases near neutral stability ($\zeta = 0$) and since the

https://doi.org/10.5194/egusphere-2025-5430
Preprint. Discussion started: 21 January 2026

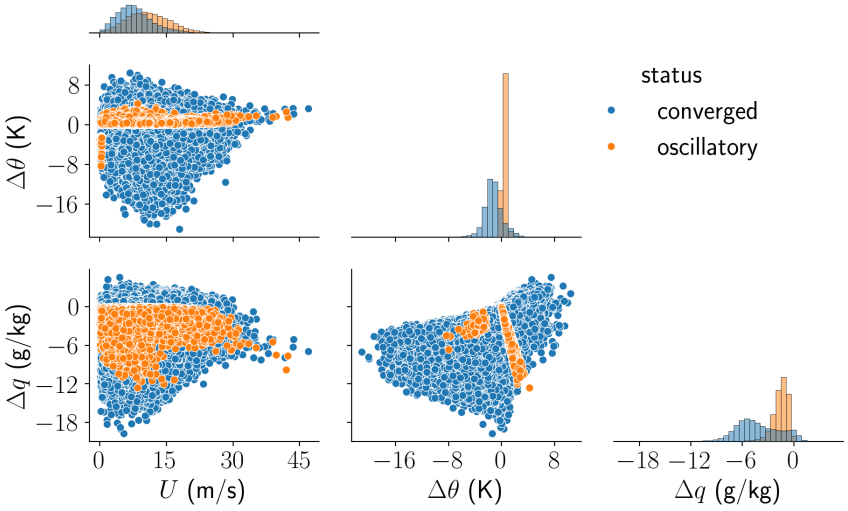

Figure 3. A corner plot showing histograms and pairwise scatter plots of the variables U, $\Delta\theta$, and Δq for both atmospheric conditions that produce oscillatory, non-convergent iterations and those whose iteration converges to a solution. Histograms are normalized so that the heights of bars in different case categories sum to the same value. The U, $\Delta\theta$, and Δq samples used here are 10 years of daily instantaneous output from the CTRL simulation. The classification ("converged" versus "oscillatory") was done in offline calculations using Alg. 1 and 1000 iterations.

stability is controlled in part by U, $\Delta\theta$, and Δq, normalized histograms of U, $\Delta\theta$, and Δq values are provided in the main diagonal of Fig. 3 for both data points with oscillations and data points that have converged to a solution. Off-diagonal entries show the pairwise scatter plots of U, $\Delta\theta$, and Δq for each class of data. The main condition for which there is usually a lack of convergence in the solution of Eq. (13) is approximately $0\ \text{K} < \Delta\theta < 0.7\ \text{K}$. Having identified this condition, we explore in which geographical locations and how often the CTRL simulation exhibits this condition. Fig. 4 shows the percentage of days in which $0\ \text{K} < \Delta\theta < 0.7\ \text{K}$ for the months of December, January, and February (hereinafter DJF) as well as June, July, and August (hereinafter JJA) averaged over the 10 years of output from the CTRL simulation. In DJF, the most frequent occurrences (>8%) of these conditions are in the Southern Ocean along the ice edge. Higher frequencies are also found in the mid-latitude storm tracks over the North Atlantic and Pacific Oceans. In JJA, the most frequent occurrences (>8%) are over the North Atlantic and Pacific just south of the ice edge, as well as over the Arabian Sea.

3.3 Regularization of heat exchange coefficient to recover solution existence

To enforce continuity of the heat exchange coefficient C_{HN}, we propose a standard C^k regularization which replaces the jump discontinuity with a polynomial function $p^{(k)}_{\varepsilon_{\text{reg}}}$ with two parameters k (a non-negative integer) and ε_{reg} (a small positive value).

https://doi.org/10.5194/egusphere-2025-5430
Preprint. Discussion started: 21 January 2026

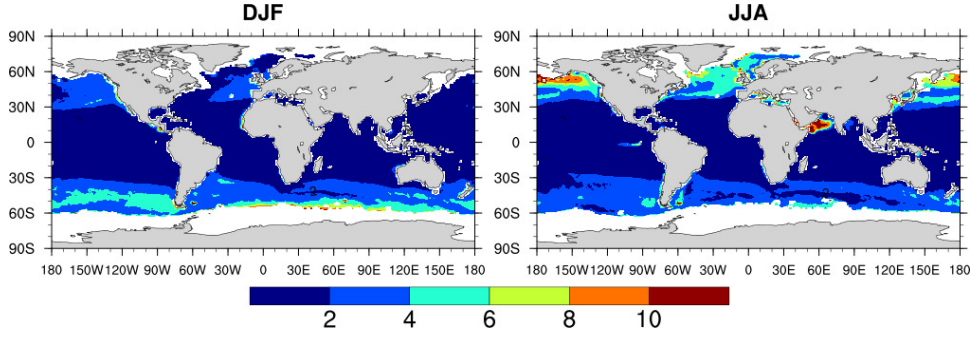

Figure 4. Percentage of days for which the daily instantaneous output of $\Delta\theta$ in DJF (left) or JJA (right) falls in the range of 0 K to 0.7 K in 10 years of the CTRL simulation, which, as indicated by Fig. 3, is the main condition under which an oscillatory iteration is most likely. Gray shading indicates land, and white areas are sea ice.

The new regularized coefficient, which we denote by $\widehat{C}^{(k)}_{\mathrm{HN},\varepsilon_{\mathrm{reg}}}$, has k continuous derivatives and is defined by

$$\widehat{C}^{(k)}_{\mathrm{HN},\varepsilon_{\mathrm{reg}}}(\zeta) := \begin{cases} 0.0327, & \zeta \leqslant -\varepsilon_{\mathrm{reg}} \\ p^{(k)}_{\varepsilon_{\mathrm{reg}}}(\zeta), & -\varepsilon_{\mathrm{reg}} < \zeta \leqslant \varepsilon_{\mathrm{reg}} \\ 0.018, & \zeta > \varepsilon_{\mathrm{reg}}. \end{cases} \tag{21}$$

In turn, $\widehat{C}^{(k)}_{\mathrm{HN},\varepsilon_{\mathrm{reg}}}$ is used to derive a regularized version of the exchange coefficient $\widehat{C}_{\mathrm{H}}$, which we denote by $\widehat{C}^{(k)}_{\mathrm{H},\varepsilon_{\mathrm{reg}}}$ and which will take the place of $\widehat{C}_{\mathrm{H}}$ in Eq. (13). Details on the construction of the polynomial $p^{(k)}_{\varepsilon_{\mathrm{reg}}}$ and the regularized exchange coefficient $\widehat{C}^{(k)}_{\mathrm{H},\varepsilon_{\mathrm{reg}}}$ are provided in Appendix C. Fig. 5 provides a visualization of the polynomial $p^{(0)}_{\varepsilon_{\mathrm{reg}}}$, which corresponds to the case of linear interpolation. Higher-order regularizations which preserve continuity of first and second derivatives are not necessary for the fixed-point iterations used in E3SMv2 which require no information on the derivatives of $\boldsymbol{f}$. We thus use only the polynomial $p^{(0)}_{\varepsilon_{\mathrm{reg}}}$ in Eq. (21) in the rest of this work. However, if higher-order fixed-point solvers are desired, then commensurately higher-order regularizations corresponding to the polynomials $p^{(1)}_{\varepsilon_{\mathrm{reg}}}$ and even $p^{(2)}_{\varepsilon_{\mathrm{reg}}}$ may be required. Details on the construction of these regularizations are provided in Appendix C for the interested reader.

The regularization parameter $\varepsilon_{\mathrm{reg}}$ determines how much of the original exchange coefficient C_{HN} is replaced by the polynomial $p^{(k)}_{\varepsilon_{\mathrm{reg}}}$. In principle, any positive value of $\varepsilon_{\mathrm{reg}}$ ensures that $\boldsymbol{f}$ is continuous and thus, the turbulent flux parameterization in Eq. 13 has a solution. In practice, smaller values of $\varepsilon_{\mathrm{reg}}$ will preserve more of the original exchange coefficient in Large and Pond (1982) but may not alleviate the problem of oscillating iterations due to the sharp gradient at $\zeta = 0$, an issue which we highlight in Sect. 3.4. In contrast, larger values of $\varepsilon_{\mathrm{reg}}$ make it easier for numerical methods to converge to a solution of the regularized equation but modify more of the original exchange coefficient. Thus, care must be taken in choosing $\varepsilon_{\mathrm{reg}}$ so that desirable features of the original exchange coefficient are preserved while also not making it onerously difficult for iterative methods to converge to a solution. A comparison of the convergence of the iterative method as well as differences in the computed turbulent fluxes for various values of $\varepsilon_{\mathrm{reg}}$ is provided in Appendix C. Based on these results, we recommend a value of

https://doi.org/10.5194/egusphere-2025-5430
Preprint. Discussion started: 21 January 2026

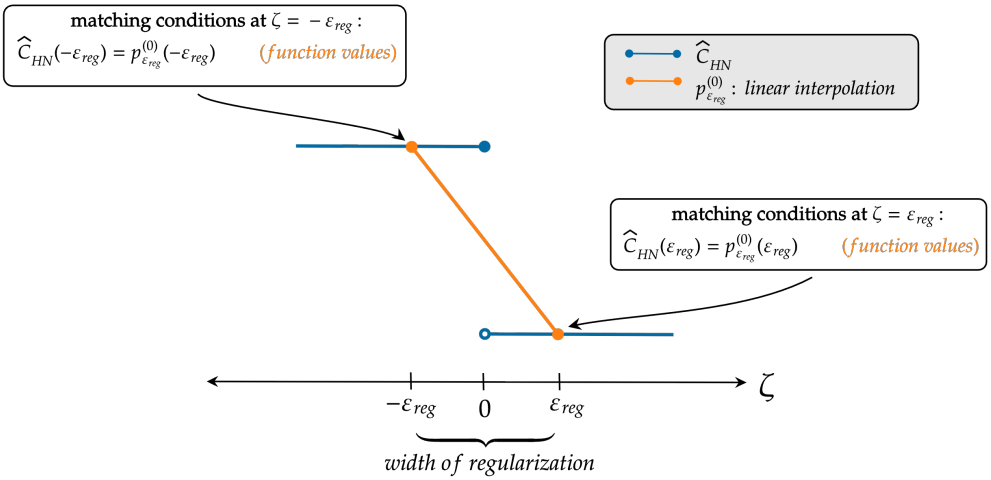

Figure 5. Neutral exchange coefficient of heat $\widehat{C}_{\mathrm{HN}}$ and its continuous regularization using linear interpolation, $p^{(0)}_{\varepsilon_{\mathrm{reg}}}$. Continuity is enforced by matching the interpolant to the values of $\widehat{C}_{\mathrm{HN}}$ at the endpoints of the region of regularization given by $-\varepsilon_{\mathrm{reg}} \leqslant \zeta \leqslant \varepsilon_{\mathrm{reg}}$.

$\varepsilon_{\mathrm{reg}} = 0.1$, which produces turbulent fluxes that do not differ significantly from the fluxes produced when using a regularization with smaller values of $\varepsilon_{\mathrm{reg}}$.

3.4 Ensuring convergent iteration for the regularized system

While the goal of the regularization in Sect. 3.3 is to ensure that the system Eq. (13) has at least one solution for iterative methods to converge to, the potentially sharp gradient (depending on how small the regularization parameter $\varepsilon_{\mathrm{reg}}$ is) introduced in the regularization can pose issues for iterative methods such as the fixed-point and nonlinear Gauss-Seidel iterations. In particular, the presence of sharp gradients often necessitates the use of damping (i.e. $\alpha < 1$ in Eq. (16)) to reduce the iteration "step size" and prevent over and under-shooting of iterates. To see this, we apply a variant of the default iteration described in Alg. 1 that (i) takes a fixed 100 iterations and (ii) introduces a damping parameter $0 < \alpha < 1$ to compute the solution of the regularized turbulent flux parameterization in Eq. (C3) with $\varepsilon_{\mathrm{reg}} = 0.1$ for the example described by Eq. (20). We consider the damping parameters $\alpha = 1$, 0.5, and 0.1 and show the results in Fig. 6. It is clear that the damped iteration converges to the solution of the regularized Eq. (C3) so long as the damping parameter is chosen small enough. In particular, if α is too large relative to $\varepsilon_{\mathrm{reg}}$, the oscillations are still present at varying levels depending on the value of α chosen. In the F2010 simulations described in Sect. 2.2, we fix $\varepsilon_{\mathrm{reg}} = 0.1$ and $\alpha = 0.016$, which allows convergence of the iterations for all meteorological conditions encountered in the 10-year model run according to the convergence criteria discussed next in Sect. 3.5.

3.5 Number of iterations and stopping criterion

Before presenting the full algorithm for numerically solving the regularized turbulent flux parameterization in Eq. (C3), we discuss convergence criteria for terminating the iterative process. The default E3SM iteration described in Alg. 1 takes two it-

https://doi.org/10.5194/egusphere-2025-5430
Preprint. Discussion started: 21 January 2026

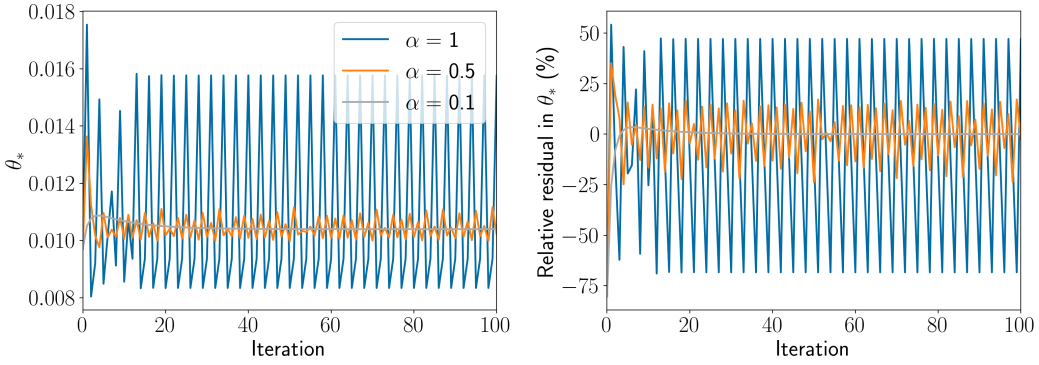

Figure 6. The iterate $(\theta_*)_n$ and its relative residual $|\boldsymbol{f}\left((u_*)_n, (u_{10N})_n, (\theta_*)_n, (q_*)_n\right) - (\theta_*)_n|/|(\theta_*)_n + \epsilon_3|$ when approximating the solution of the regularized turbulent flux parameterization in Eq. (C3) with conditions described by Eq. (20). The value of the regularization parameter is $\varepsilon_{\text{reg}} = 0.1$. The iterates are described by Alg. 2 with damping parameters chosen from $\alpha \in \{1, 0.5, 0.1\}$.

erations and returns the second iterate as the approximation to the scaling parameters. Standard practice in numerical methods is to have iterative methods, such as the fixed-point iteration, terminate when a convergence test is passed or after a maximum number of iterations `maxiter` is reached (chosen to be orders of magnitude larger than is expected for the iteration to converge).

We utilize the same relative residual as in Sect. 3.2, i.e. Eq. (19). Given the iterate $\boldsymbol{x}_n = ((u_*)_n, (u_{10N})_n, (\theta_*)_n, (q_*)_n)^T$, the proposed convergence test is to check whether $\mathcal{R}(\boldsymbol{x}_n; \boldsymbol{\xi}) < \texttt{tol}$ for a user-prescribed tolerance $\texttt{tol} > 0$. The full algorithm for approximating the scaling parameters described by the turbulent flux parameterization in Eq. (C3) is given in Alg. 2. For the 10-year simulation SENS described in Sect. 2.5, we take $\texttt{tol} = 10^{-4}$ and $\texttt{maxiter} = 2 \times 10^6$.

To demonstrate the efficacy of the regularized neutral exchange coefficient in removing oscillations in the iterate $\boldsymbol{x}_n$, we perform an offline test on the same 10 years of daily instantaneous output from the CTRL simulation shown in Fig. 3, this time using Alg. 2. The corresponding corner plot showing classifications of each data point as oscillatory or convergent is presented in Fig. 7. We observe that all sets of meteorological conditions are now able to be driven to the desired residual error tolerance, from which we surmise that the regularization proposed in Sect. 3.3 is sufficient in addressing solution non-existence in the Large and Pond parameterization.

3.6 Comments on computational cost

Finally, we briefly comment on the efficiency of the proposed Alg. 2 compared to the E3SMv2 default Alg. 1. One should not generally expect to obtain a high level of accuracy in the scaling parameters (and hence, the turbulent fluxes as well) using the default two iterations described in Alg. 1. On the one hand, developers of E3SM and other ESMs might argue that the level of accuracy achieved with two iterations is on par with the low level of accuracy associated with many other numerical calculations of E3SM, for instance, first-order time integration and coupling methods (Wan et al., 2021, 2015). On the other hand, recent explorations of more accurate time integration techniques for the resolved atmospheric dynamics (Vogl et al.,

https://doi.org/10.5194/egusphere-2025-5430
Preprint. Discussion started: 21 January 2026

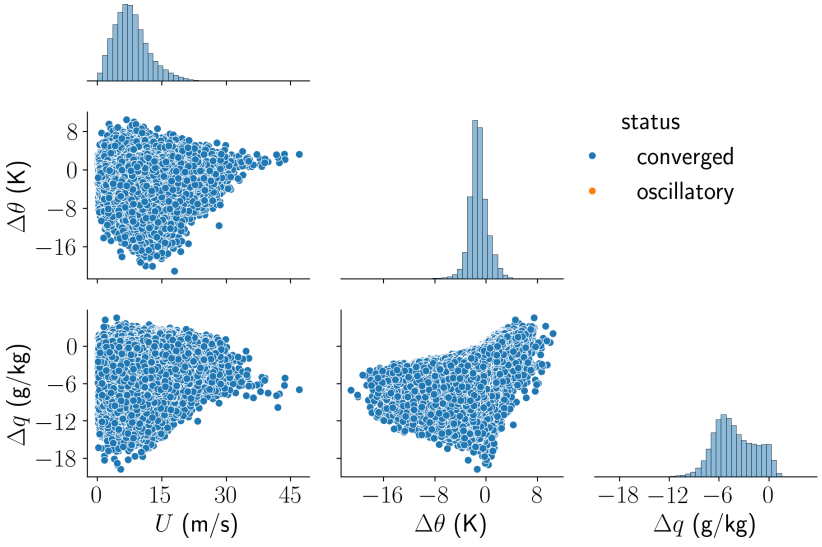

Figure 7. A corner plot showing the histograms and pairwise scatter plots of the variables U, $\Delta\theta$, and Δq for both atmospheric conditions that produce oscillatory, non-convergent iterations and those whose iteration converges to a solution in the regularized parameterization described in Sect. 3.3. Histograms are normalized along the diagonal so that the heights of the bars for each group sum to the same value. The U, $\Delta\theta$, and Δq samples used here are 10 years of daily instantaneous output from the CTRL simulation. The classification ("converged" versus "oscillatory") was done in offline calculations using the regularized Alg. 2 with $\varepsilon = 0.1$, $\alpha = 0.016$, and $\texttt{tol} = 10^{-4}$. The corresponding results without regularization can be found in Fig. 3.

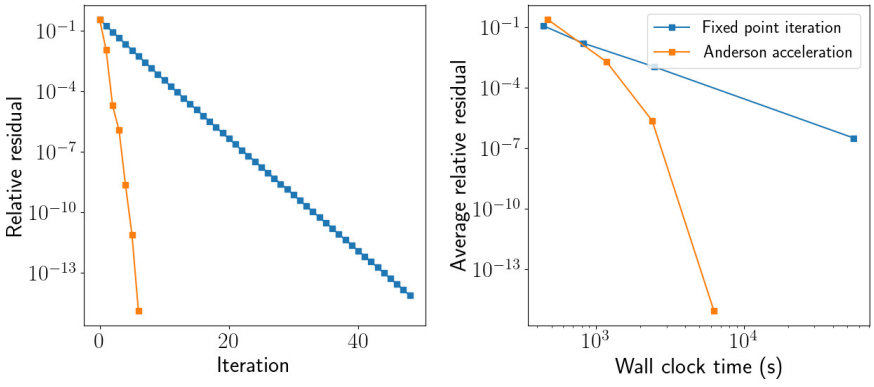

Figure 8. A demonstration of Anderson acceleration to improve convergence of scaling parameters. (left) Behavior of the relative residual $\mathcal{R}(\boldsymbol{x}_n; \boldsymbol{\xi})$ for approximating surface fluxes from the parameterization Eq. (C3) at a single location with $\texttt{maxiters} = 100$ and $\texttt{tol} = 10^{-14}$. (right) Average residual for meteorological conditions sampled across a year of data from the CTRL simulation vs. wall clock time. Individual points correspond to fixed-point and Anderson acceleration iterations with $\texttt{maxiters} = 2, 5, 10, 100$ and $\texttt{tol} = 10^{-14}$.

https://doi.org/10.5194/egusphere-2025-5430
Preprint. Discussion started: 21 January 2026

2019; Gardner et al., 2018) in conjunction with improvements to physics parameterizations and their coupling (Wan et al., 2024; Zhang et al., 2023b) in ESMs means that the relatively large approximation errors associated with Alg. 1 may start to exceed errors in the other parts of E3SM in future versions of this ESM.

While Alg. 2 is usually (depending on the value of `tol`) more computationally expensive than the default E3SMv2 algorithm since more than two iterations are usually required to reach a given tolerance, techniques for accelerating convergence of Alg. 2 are readily available. For example, Anderson acceleration (Anderson, 1965) updates the iteration by computing a linear combination of m previous iterates and, in many cases, converges faster than the standard fixed-point and Gauss-Seidel iterations. Efficient implementations are available to Fortran and `C++` codes via software libraries such as SUNDIALS (Hindmarsh et al., 2005; Gardner et al., 2022). To demonstrate the potential benefits of Anderson acceleration, we solve the equations underlying the regularized turbulent flux parameterization Eq. (C3) in offline calculations using Earth system conditions sampled from the CTRL simulation every five days over the course of one year. Numerical solution of the scaling parameter equations is done using either (i) Anderson acceleration from SUNDIALS with $m = 1$ which computes the update $\boldsymbol{x}_{n+1}$ using the previous iterates $\boldsymbol{x}_n$ and $\boldsymbol{x}_{n-1}$, or (ii) the standard fixed-point iteration Eq. (16) which has the same computational cost per iteration as the default E3SM iteration in Alg. 1 (Fig. 8). We observe that Anderson acceleration converges rapidly and also results in significant speed-up in wall clock time in comparison to the standard fixed-point iteration. For instance, Anderson acceleration attains an average relative residual of 10^{-4} more than three times faster than the standard fixed-point iteration.

4 Analyzing and addressing uniqueness issues for the scaling parameters

With some confidence that a solution now exists to the regularized Large and Pond parameterization described in Sect. 3.3 and its corresponding algorithm in Alg. 2, we now turn our attention to the issue of solution uniqueness. If the underlying equations have more than one solution, then the iterative method described in Alg. 2 may converge to different solutions depending on the initial guess.

4.1 Unbounded Obukhov stability parameter produces unintended solution

In this subsection, we demonstrate that the principal driver of solution non-uniqueness is a singularity in the Obukhov stability parameter ζ defined in Eqs. (7) and (11). In particular, due to the presence of u_* in its denominator, ζ is undefined when $u_* = 0$. Likewise, the function $\boldsymbol{f}$ describing the right-hand side of Eq. (13) depends on ζ and is also undefined when $u_* = 0$. From a practical perspective, this also means that small values of u_* may potentially cause ζ to take on extremely large magnitudes. The remainder of this section shall be divided into two parts: in Sect. 4.1.1 we provide a mathematical description of expected outcomes in the case when $u_* = 0$, while in Sect. 4.1.2 we relate the mathematical analysis to the observed outcomes of iterative methods such as those in Algs. 1 and 2 in light of the aforementioned undefined behavior.

https://doi.org/10.5194/egusphere-2025-5430
Preprint. Discussion started: 21 January 2026

Algorithm 2 Regularized atmosphere-ocean iteration.

Input: Bulk variables $\boldsymbol{\xi} = (U, \theta_a, \theta_s, z, \rho_a, q_a, q_s)^T$; limiting parameter ζ_{max}; damping parameter $\alpha \in (0, 1]$; tolerance `tol`; maximum iterations `maxiter`.

Output: Approximation $(u_*)_n$, $(u_{10\text{N}})_n$, $(\theta_*)_n$, and $(q_*)_n$ to the turbulent flux parameterization Eq. (C3).

function REGULARIZEDITERATION($\boldsymbol{\xi}$, ζ_{max}, α, `tol`, `maxiter`)

Set $n = 0$.

Compute the initial estimate based on neutral conditions:

$$
\begin{aligned}
(u_{10\text{N}})_n &= U\,, \\
(u_*)_n &= \sqrt{C_{\text{DN}}(U)} \cdot U\,, \\
(\theta_*)_n &= \widehat{C}_{\text{HN}}(\Delta\theta) \cdot \Delta\theta\,, \\
(q_*)_n &= \widehat{C}_{\text{EN}} \cdot \Delta q.
\end{aligned}
$$

Compute limited stability parameter $\tilde{\zeta}_0 = \tilde{\zeta}\Big((u_*)_0, (\theta_*)_0, (q_*)_0; \zeta_{\text{max}}\Big)$ according to Eq. (17).

while $\mathcal{R}\Big((u_*)_n, (u_{10\text{N}})_n, (\theta_*)_n, (q_*)_n; \boldsymbol{\xi}\Big) >$ `tol` **do**

$n \leftarrow n + 1$.

Update 10-m neutral wind speed:

$$
(u_{10\text{N}})_n = \alpha \frac{\widehat{C}_{\text{D}}\Big((u_{10\text{N}})_{n-1}, \tilde{\zeta}_{n-1}; \boldsymbol{\xi}\Big)}{\sqrt{C_{\text{DN}}\Big((u_{10\text{N}})_{n-1}\Big)}} \cdot U + (1-\alpha) \cdot (u_{10\text{N}})_{n-1}.
$$

Apply updated 10-m neutral wind speed to simultaneously update scaling parameters using regularized coefficients:

$$
\begin{pmatrix} (u_*)_n \\ (\theta_*)_n \\ (q_*)_n \end{pmatrix} = \alpha \begin{pmatrix} \widehat{C}_{\text{D}}\Big((u_{10\text{N}})_n, \tilde{\zeta}_{n-1}; \boldsymbol{\xi}\Big) \cdot U \\ \widehat{C}^{(0)}_{\text{H},\varepsilon_{\text{reg}}}\Big((u_{10\text{N}})_n, \tilde{\zeta}_{n-1}; \boldsymbol{\xi}\Big) \cdot \Delta\theta \\ \widehat{C}_{\text{E}}\Big((u_{10\text{N}})_n, \tilde{\zeta}_{n-1}; \boldsymbol{\xi}\Big) \cdot \Delta q \end{pmatrix} + (1-\alpha) \begin{pmatrix} (u_*)_{n-1} \\ (\theta_*)_{n-1} \\ (q_*)_{n-1} \end{pmatrix}.
$$

Update stability parameter $\tilde{\zeta}_n = \tilde{\zeta}\Big((u_*)_n, (\theta_*)_n, (q_*)_n; \zeta_{\text{max}}\Big)$.

if $n >$ `maxiter` **then**

ERROR("Maximum iterations reached without achieving desired tolerance.")

end if

end while

return $(u_*)_n, (\theta_*)_n, (q_*)_n$.

4.1.1 Theoretical analysis of iterate convergence to wrong solution

While ζ is undefined whenever $u_* = 0$, we may still gain understanding of the behavior of ζ by examining the limiting behavior as $u_* \to 0$. It is important to note that ζ is also a function of θ_* and q_*, whose values will also vary throughout the application

https://doi.org/10.5194/egusphere-2025-5430
Preprint. Discussion started: 21 January 2026

of an iterative method. For reasons that will become apparent in Sect. 4.1.2, we shall consider the multivariable limiting behavior $\lim_{(u_*,\theta_*,q_*)\to(0,0,0)} \zeta(u_*,\theta_*,q_*)$, where, in addition to $u_* \to 0$, we are also interested in the case when θ_* and q_* simultaneously approach 0.

In what may seem like a purely academic exercise at first, we demonstrate that the limiting behavior of ζ is different depending on the trajectory taken towards $(u_*,\theta_*,q_*) = (0,0,0)$. We will express u_*, θ_*, and q_* using a dummy variable s so that the limiting behavior may be examined as $s \to 0$ instead — that is, $\lim_{(u_*,\theta_*,q_*)\to(0,0,0)} \zeta(u_*,\theta_*,q_*) = \lim_{s\to 0} \zeta(u_*(s),\theta_*(s),q_*(s))$.

A basic result from multivariable calculus states that the limit of a multivariable function as its input variables approach a particular point exists if and only if the function approaches the same value along every trajectory that approaches the particular point. We show here that it is possible to construct two trajectories along which ζ converges to different values, and explain the expected implication of each case on the turbulent flux algorithms 1 and 2.

1. The first trajectory is described by $u_*(s) = s^{3/2}$, $\theta_*(s) = s$, and $q_*(s) = s$. By evaluating the limit along this trajectory using Eq. (7) and the definition of the trajectory, we can see that $\lim_{s\to 0} \zeta(u_*(s),\theta_*(s),q_*(s)) = +\infty$. Whenever $\zeta \to +\infty$, we can see by inspection of the stability functions $\psi_{(\mathrm{m,h,q})}$ (see Eqs. (A4)-(A5)) and exchange coefficients $\widehat{C}_{(\mathrm{D,H,E})}$ (see Eqs. (A1)-(A3) and their regularized variants in Eq. (A11)) that the right-hand side of the turbulent flux parameterization Eq. (13) approaches 0. In other words, along this kind of trajectory, the residual of Eq. (13) decays to 0. We expect that numerically, $(u_*,\theta_*,q_*) = (0,0,0)$ serves as a secondary "solution" that iterative methods may converge to if they approach a trajectory such as the one described here.

2. The second trajectory is described by $u_*(s) = s$, $\theta_*(s) = s^3$, and $q_*(s) = s^3$, from which we see that $\lim_{s\to 0} \zeta(u_*(s),\theta_*(s),q_*(s)) = 0$. In other words, the right-hand side of Eq. (13) is finite and nonzero, and the residual of Eq. (13) does not decay to 0. This case demonstrates the existence of trajectories along which iterative methods will *not* converge to $(u_*,\theta_*,q_*) = (0,0,0)$.

In summary, the Obukhov stability parameter may become unbounded due to division by u_* in its definition. When iterations produced by iterative methods fall along certain trajectories, we expect that they may converge to $(u_*,\theta_*,q_*) = (0,0,0)$, which serves as a secondary "solution" to Eq. (13). However, according to the multivariate calculus result stated earlier, because ζ can approach distinct values (e.g., $+\infty$ and 0) when different trajectories are taken towards $(u_*,\theta_*,q_*) = (0,0,0)$, the point $(u_*,\theta_*,q_*) = (0,0,0)$ is *not* an actual solution to Eq. (13), hence it is problematic that an iterative method may converge to this point. Furthermore, it is worth noting that the danger of converging to $(u_*,\theta_*,q_*) = (0,0,0)$ can be seen from the continuous formulation of the parameterization; hence, using a different numerical algorithm might not automatically avoid this danger unless deliberate design features are introduced, as we discuss below in Sect. 4.4.

4.1.2 Numerical example of convergence to unintended solution

We now use offline calculations to demonstrate that certain meteorological conditions indeed result in the situation of iterative methods being able to converge to two different solutions depending on how the initial iterate is chosen. An example of such

https://doi.org/10.5194/egusphere-2025-5430
Preprint. Discussion started: 21 January 2026

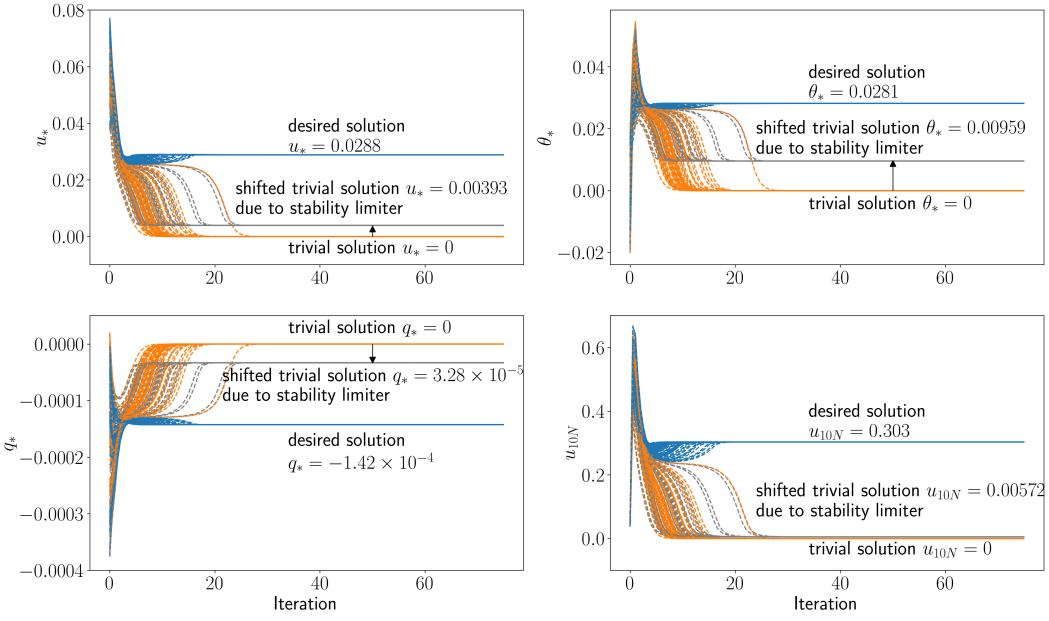

Figure 9. Progress of approximating the scaling parameters u_*, θ_*, and q_* and 10-m wind speed, $u_{10\mathrm{N}}$, in Alg. 2 with and without stability limiter. Each dashed line represents an application of Algorithm 2 with an initial guess drawn randomly from a uniform distribution. Without the limiter, the iterations converge to one of two solutions depending on the initial guess: a trivial one at $(u_*, u_{10\mathrm{N}}, \theta_*, q_*) = (0,0,0,0)$ and a non-trivial solution $(u_*, u_{10\mathrm{N}}, \theta_*, q_*) = (0.0288, 0.303, -0.000142, 0.0281)$. When the limiter is applied with $\zeta_{\max} = 10$, as is currently done in E3SM, the trivial solution at $(u_*, u_{10\mathrm{N}}, \theta_*, q_*) = (0,0,0,0)$ is shifted to $(u_*, u_{10\mathrm{N}}, \theta_*, q_*) = (0.00393, 0.00959, -3.28 \times 10^{-5}, 0.00572)$.

meteorological conditions for which it is possible that the iterates $\left((u_*)_n, (u_{10\mathrm{N}})_n, (\theta_*)_n, (q_*)_n\right) \to (0,0,0,0)$ is

$$U = 0.1 \text{ m/s}, \quad z = 13.43 \text{ m}, \quad \theta_s = 300.04 \text{ K}, \quad \theta_a = 301.78 \text{ K}, \quad q_a = 16.87 \text{ g/kg}. \tag{22}$$

We apply Alg. 2 100 times without the stability limiter (i.e. $\tilde{\zeta}$ is replaced by ζ in Alg. 2), each with a randomized initial iterate, and plot the scaling parameters at each iteration of the algorithm (Fig. 9). We observe convergence of the iterates to two distinct points for this example — one at $(u_*, u_{10\mathrm{N}}, \theta_*, q_*) = (0,0,0,0)$ corresponding to the case when $\zeta \to \pm\infty$ and another at $(u_*, u_{10\mathrm{N}}, \theta_*, q_*) = (0.0288, 0.303, 0.0281, -0.000142)$. Such behavior shows the importance of preventing $\zeta \to \pm\infty$ for the regularized turbulent flux parameterization Eq. (C3), and it supports the idea of limiting ζ in general, although we shall elaborate in the next subsection that the limiter needs to be implemented in a careful way in order to be effective and reliable. We also note that while this issue also persists for the default unregularized parameterization Eq. (13), the experiment presented in Fig. 9 is performed with the regularized turbulent flux parameterization in order to ensure that issues with solution existence are not encountered.

https://doi.org/10.5194/egusphere-2025-5430
Preprint. Discussion started: 21 January 2026

4.2 Role of Obukhov stability limiter in solution non-uniqueness

We now turn our attention to the limited stability parameter $\tilde{\zeta}$ and address its role in determining uniqueness of the surface fluxes. Recall that E3SM utilizes the stability limiter (i.e., Eq. 17) in the implementation of Alg. 1 to prevent the magnitude of ζ from growing to physically unreasonable values but also prevents the scenario where $\zeta \to \pm\infty$. To the best of our knowledge, no systematic analysis has been carried out to determine the effect of the limiter (17) on convergence of Alg. 1.

One might expect that since the limiter removes the possibility that $\zeta \to \pm\infty$, iterative methods should not be able to converge to $(u_*, u_{10\mathrm{N}}, \theta_*, q_*) = (0,0,0,0)$, and Eq. (C3) should have a unique solution when the limiter is applied. However, we demonstrate that while the limiter does prevent convergence of the iterates to $(u_*, u_{10\mathrm{N}}, \theta_*, q*) = (0,0,0,0)$, it introduces a shifted "solution" to the system. To see this, we consider the same example described by Eq. (22) but apply the limiter (17) with $\zeta_{max} = 10$ as in E3SMv2 (Fig. 9). We observe that the "solution" at $(u_*, u_{10\mathrm{N}}, \theta_*, q_*) = (0,0,0,0)$ is shifted to $(u_*, u_{10\mathrm{N}}, \theta_*, q_*) = (0.00393, 0.00959, -3.28 \times 10^{-5}, 0.00572)$ and in fact, the regularized turbulent flux parameterization described by Eq. (C3) has two solutions when the stability limiter is applied.

4.3 Exploring the solution space via bifurcation diagrams

More generally, the value of the limiting parameter $\zeta_{\max}$ has a strong effect on the number of solutions of Eq. (C3). When an analytic solution of a given equation is known, a systematic analysis of the effect of a model parameter on uniqueness of the solution is straightforward. For instance, one can express the solution as a function of the parameter of interest and generate a *bifurcation diagram* (Chow and Hale, 2012) which provides qualitative information on the solution for each value of the parameter. Given that an analytic solution of Eq. (C3) is not known, an approximate bifurcation diagram may still be generated by performing several runs of Alg. 2 for a range of different initial guesses and observing how many distinct solutions the algorithm converges to for different values of $\zeta_{\max}$.

With E3SM's default of $\zeta_{\max} = 10$ in mind, we examined a large number of meteorological conditions in the CTRL simulation while varying $\zeta_{\max}$ over a range of values from 10^{-1} to 10^4. Based on this analysis, we observed four distinct scenarios regarding solution uniqueness. These scenarios are illustrated in Fig. 10 alongside examples of the meteorological conditions producing those scenarios. An in-depth explanation of these scenarios is provided below.

1. There is exactly one solution which does not depend on $\zeta_{\max}$.

https://doi.org/10.5194/egusphere-2025-5430
Preprint. Discussion started: 21 January 2026

Scenario/Bifurcation	Description
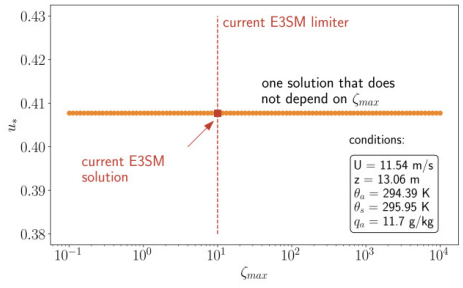	There is exactly one solution which is independent of $\zeta_{\max}$.
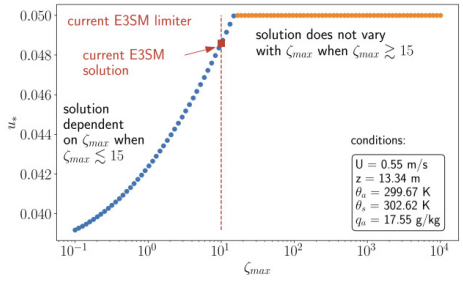	There is exactly one solution which varies with $\zeta_{\max}$ whenever $\zeta_{\max} \lesssim 15$ and does not vary with $\zeta_{\max}$ whenever $\zeta_{\max} \gtrsim 15$. To isolate the desired solution which does not vary with the limiter, the limiting parameter $\zeta_{\max}$ must be chosen sufficiently large.
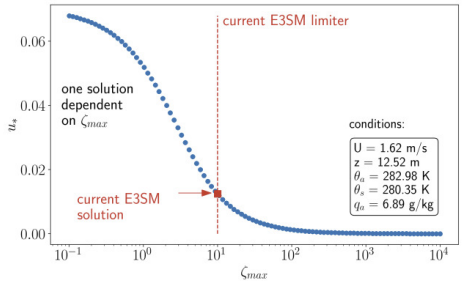	There is exactly one solution which always varies with $\zeta_{\max}$. It is unclear if the desired solution is in this scenario. The limiting parameter is left unadjusted.
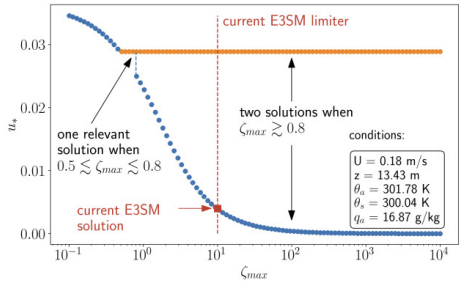	There is a bifurcation point at which the underlying equations transition from having exactly one solution to having two solutions. When two solutions exist, one of them varies with $\zeta_{\max}$ while the other does not. When one solution exists, it may vary with $\zeta_{\max}$ (e.g. for $\zeta_{\max} \lesssim 0.5$) or may be constant with $\zeta_{\max}$ (e.g. for $0.5 \lesssim \zeta_{\max} \lesssim 0.8$)

Figure 10. Four different possible scenarios arising from use of limiters on the Obkuhov stability parameter. Detailed discussions can be found in Sect. 4.3.

https://doi.org/10.5194/egusphere-2025-5430
Preprint. Discussion started: 21 January 2026

2. There is exactly one solution which varies with $\zeta_{\max}$ until a turning point after which the solution is constant with $\zeta_{\max}$. When the solution varies with $\zeta_{\max}$, it is described implicitly by the manifold on which $|\zeta| = \zeta_{\max}$:

$$\begin{cases} u_*(\zeta_{\max}) = \widehat{C}_{\mathrm{D}}\left(u_{10\mathrm{N}}(\zeta_{\max}), \zeta_{\max} \cdot \operatorname{sgn}(\Delta\theta); \boldsymbol{\xi}\right) \cdot U \\ u_{10\mathrm{N}}(\zeta_{\max}) = \dfrac{\widehat{C}_{\mathrm{D}}\left(u_{10\mathrm{N}}(\zeta_{\max}), \zeta_{\max} \cdot \operatorname{sgn}(\Delta\theta); \boldsymbol{\xi}\right)}{\sqrt{C_{\mathrm{DN}}\left(u_{10\mathrm{N}}(\zeta_{\max})\right)}} U \\ \theta_*(\zeta_{\max}) = \widehat{C}^{(k)}_{\mathrm{H},\varepsilon_{\mathrm{reg}}}\left(u_{10\mathrm{N}}(\zeta_{\max}), \zeta_{\max} \cdot \operatorname{sgn}(\Delta\theta)); \boldsymbol{\xi}\right) \cdot \Delta\theta \\ q_*(\zeta_{\max}) = \widehat{C}_{\mathrm{E}}\left(u_{10\mathrm{N}}(\zeta_{\max}), \zeta_{\max} \cdot \operatorname{sgn}(\Delta\theta); \boldsymbol{\xi}\right) \Delta q. \end{cases} \tag{23}$$

3. There is exactly one solution which depends on $\zeta_{\max}$. This solution is given implicitly by Eq. (23).

4. For $\zeta_{\max}$ within a certain range, there are exactly two solutions, one of which does not vary with $\zeta_{\max}$ and one of which varies with $\zeta_{\max}$. The latter is described by Eq. (23). For $\zeta_{\max}$ outside of this range, there is a unique solution which may or may not vary with $\zeta_{\max}$. The value of $\zeta_{\max}$ at which the number of possible solutions transitions from one to two is known as a *bifurcation point*.

The first scenario is ideal in the sense that the limiter has no effect on the solution. While a rigorous theory establishing precisely when this scenario occurs is beyond the mathematical techniques described in this paper, we suspect that this scenario may occur when the meteorological conditions prevent the stability parameter ζ from taking on large values during the iteration.

The second scenario illustrates that the limiter must be chosen carefully in order to ensure that the obtained solution exhibits desirable behavior, namely that the obtained solution should not vary with the value of $\zeta_{\max}$. When $\zeta_{\max} \gtrsim 15$, we observe that the solution is constant with respect to $\zeta_{\max}$. It is this desired solution which a numerical method should converge to. On the other hand, if $\zeta_{\max} \lesssim 15$, we observe the undesired behavior in which the solution varies with the value of $\zeta_{\max}$. Notably, the current value of $\zeta_{\max} = 10$ in E3SM is too small in that it would result in obtaining the undesired solution.

The third scenario in which the only solution depends on the value of $\zeta_{\max}$ suggests that there is no desired solution to the turbulent flux parameterization (C3). In particular, the only solution is the shifted trivial "solution" (c.f. Fig. 9) which suggests that the Large and Pond parameterization is not valid for the range of meteorological conditions that produce this behavior. For instance, it is well known that in extremely stable conditions as $\zeta \to \infty$, the assumption of constant surface fluxes with respect to altitude is violated (Optis et al., 2016) and the Monin-Obukhov Similarity Theory that underpins the derivation of the parameterization is no longer valid.

The fourth scenario, much like the second, illustrates the importance of correctly selecting $\zeta_{\max}$ to obtain the physically relevant solution. When $\zeta_{\max} \gtrsim 0.8$, there are two solutions to the turbulent flux parameterization Eq. (C3), and Alg. 2 may converge to either solution depending on the initial guess. For the small interval $0.5 \lesssim \zeta_{\max} \lesssim 0.8$, only the desired solution that does not vary with $\zeta_{\max}$ is obtained, and this finding suggests that the value of $\zeta_{\max}$ should fall in this interval to guarantee convergence of Alg. 2 to the desired solution.

https://doi.org/10.5194/egusphere-2025-5430
Preprint. Discussion started: 21 January 2026

Lastly, the issue of the limiting parameter value dictating the number of possible solutions to the underlying equations of the Large and Pond turbulent flux parameterization is likely to cause problems with solution uniqueness in other parameterizations as well. For instance, the alternate University of Arizona parameterization (Zeng et al., 1998) was implemented into E3SMv2 as a possible alternative to the Large and Pond parameterization with the same limiters described by Eq. (17). The COAREv3 parameterization (Fairall et al., 2003), on the other hand, does not utilize limiters on the stability parameter. However, when stability limiters are not applied, one may view this as the asymptotic case when $\zeta_{\max} \to \infty$ in Fig. 11; in this case, it is still possible for the underlying equations to have two solutions (c.f. Fig. 9) although we have not explored this possibility for any parameterizations aside from that of Large and Pond.

4.4 Adaptive selection of limiting parameters

The preceding discussions in Sect. 4.2 and Sect. 4.3 suggests that there is no single value of $\zeta_{\max}$ that will ensure the existence of only one solution to the turbulent flux parameterization for all meteorological conditions. For instance, for the meteorological conditions described in the fourth scenario in Fig. 10, a value of $\zeta_{\max} = 0.6$ is appropriate but would result in obtaining an undesired solution if the same value is used for the meteorological conditions described in the second scenario in Fig. 10.

Instead, we propose utilizing an adaptive stability limiter in which the value of $\zeta_{\max}$ is permitted to vary based on the meteorological conditions. The key idea is to begin with an initial maximum value of $\zeta_{\max}$ and apply Alg. 2 to obtain a

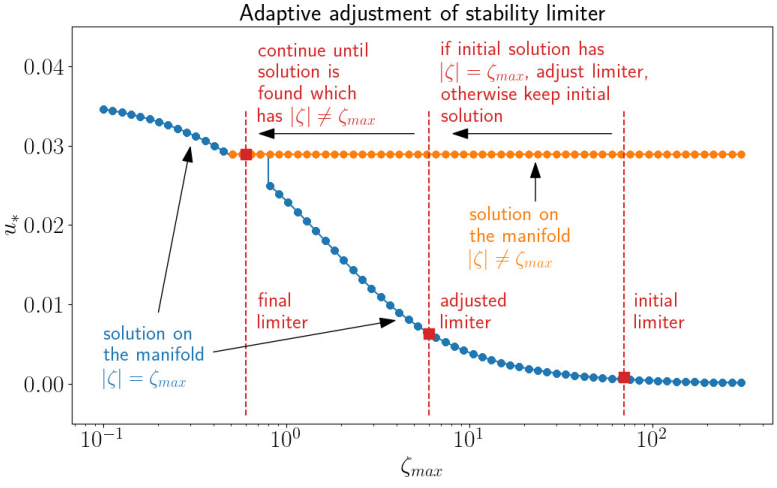

Figure 11. An example of the adaptive stability limiting process. For the initial limiter, two solutions exist — the desired solution which is constant in $\zeta_{\max}$ (orange curve) and the second, undesired solution that lies on the manifold described by $|\tilde{\zeta}| = \zeta_{\max}$ (blue curve). If the desired solution is obtained by Alg. 3, there is no need to adjust the limiting parameter $\zeta_{\max}$. Otherwise, we incrementally decrease $\zeta_{\max}$ until a solution satisfying $|\tilde{\zeta}| \neq \zeta_{\max}$ is reached. In this example, the process is guaranteed to terminate once $\zeta_{\max}$ falls in the approximate interval $(0.5, 0.8)$. In general, if the process terminates without finding the desired solution, e.g. because it does not exist (see third scenario in Fig. 10), then we default to the solution obtained from the default E3SM limiting parameter value of $\zeta_{\max} = 10$. A more detailed discussion may be found in Sect. 4.4.

https://doi.org/10.5194/egusphere-2025-5430
Preprint. Discussion started: 21 January 2026

Algorithm 3 Modified atmosphere-ocean iteration for uniqueness.

Input: Bulk variables $\boldsymbol{\xi} = (U, \theta_a, \theta_s, z, \rho_a, q_a, q_s)^T$; damping parameter $\alpha \in (0, 1]$; initial limiting parameter ζ_{max}; limiter increment $\zeta_{\text{incr}} > 0$; tolerance `tol`; maximum iterations `maxiter`.

Output: Approximation $(u_*)_n$, $(u_{10\text{N}})_n$, $(\theta_*)_n$, and $(q_*)_n$ to the turbulent flux parameterization Eq. (C3) using adaptive stability limiter.

function REGULARIZEDUNIQUEITERATION($\boldsymbol{\xi}$, ζ_{max}, ζ_{incr}, α, `tol`, `maxiter`)
  Set $\tilde{\zeta}_n = \zeta_{\text{max}}$.
  while $\tilde{\zeta}_n = \zeta_{\text{max}}$ and $\zeta_{\text{max}} > 0$ **do**
    Increment $\zeta_{\text{max}} \leftarrow \max\{\zeta_{\text{max}} - \zeta_{\text{incr}}, 0\}$.
    Call $[(u_*)_n, (\theta_*)_n, (q_*)_n]$ = REGULARIZEDITERATION($\boldsymbol{\xi}$, ζ_{max}, α, `tol`, `maxiter`).
    Compute limited stability parameter $\tilde{\zeta}_n = \tilde{\zeta}\Big((u_*)_n, (\theta_*)_n, (q_*)_n; \zeta_{\text{max}}\Big)$ according to Eq. (17).
  end while
  if $\zeta_{\text{max}} = 0$ **then**
    Set $\zeta_{\text{max}} = 10$.
    Call $[(u_*)_n, (\theta_*)_n, (q_*)_n]$ = REGULARIZEDITERATION($\boldsymbol{\xi}$, ζ_{max}, α, `tol`, `maxiter`).
  end if
return $(u_*)_n, (\theta_*)_n, (q_*)_n$.

first approximation of the scaling parameters u_*, θ_*, and q_*. If the value of the stability parameter associated with scaling parameters, $\tilde{\zeta}(u_*, \theta_*, q_*; \zeta_{\text{max}})$, is equal to ζ_{max}, we decrease the value of ζ_{max} and apply Alg. 2 until scaling parameters are obtained for which $\tilde{\zeta}(u_*, \theta_*, q_*; \zeta_{\text{max}}) \neq \zeta_{\text{max}}$. A visualization of this procedure is provided in Fig. 11. The complete turbulent flux algorithm with adaptive stability limiter is presented in Alg. 3.

When there is no desired solution, e.g. the third scenario in Fig. 10, we elect to leave the limiting parameter at its default value of $\zeta_{\text{max}} = 10$. As previously mentioned, this scenario suggests that the underlying assumptions for which the turbulent flux parameterization has been developed have been violated. This issue is a parameterization formulation problem that is beyond the scope of the present paper, which focuses on equation solvability and solution convergence.

The computational cost of Algorithm 3 is dependent on the initial value of ζ_{max}. An exploration of the sensitivity of the overall Earth system to the choice of ζ_{max} is provided in Appendix D. We only note here that the choice $\zeta_{\text{max}} = 200$ appears to be sufficient for Algorithm 3 to return scaling parameters satisfying $|\zeta| \neq \zeta_{\text{max}}$ when possible.

4.5 Occurrence of undesired solutions in E3SM

The preceding discussion highlights the issues associated with the stability limiter (17). In particular, current implementations of ocean–atmosphere turbulent flux algorithms may potentially converge to undesired solutions on the manifold $|\zeta| = \zeta_{\text{max}}$. To better understand the physical conditions producing $|\zeta| = \zeta_{\text{max}}$ when ζ_{max} is fixed at E3SMv2's value of 10, we again consider ten years of data from the CTRL simulation. We apply the default Alg. 1 with 100 iterations instead of 2 iterations and categorize each spatial location based on the value of ζ. Fig. 12 shows the distribution of meteorological conditions

https://doi.org/10.5194/egusphere-2025-5430
Preprint. Discussion started: 21 January 2026

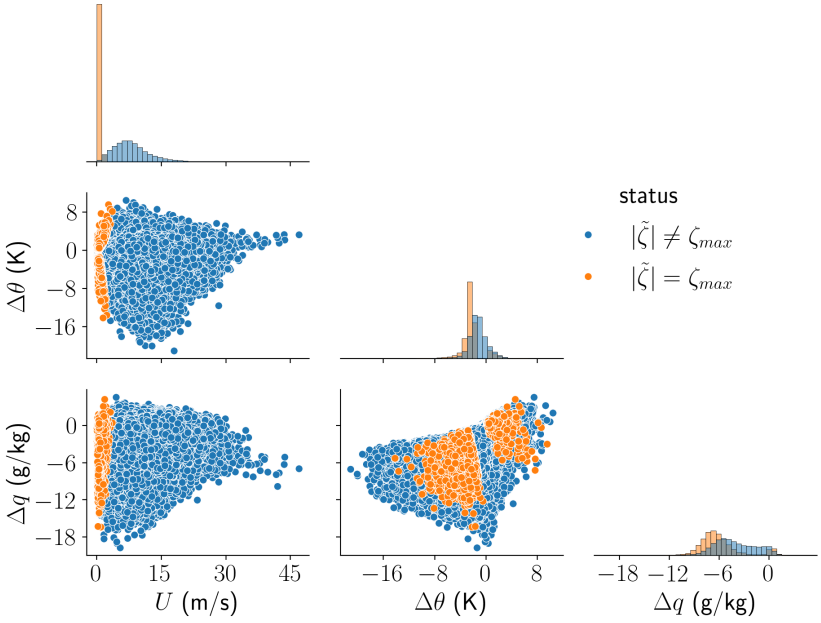

Figure 12. A corner plot similar to Fig. 3 but comparing atmospheric conditions that yield $|\tilde{\zeta}| = \zeta_{\max}$ and those that yield $|\tilde{\zeta}| \neq \zeta_{\max}$, with $\zeta_{\max}$ fixed at E3SMv2's value of 10. Further details can be found in Sect. 4.5.

when $|\zeta| = \zeta_{\max} = 10$ and when $|\zeta| \neq \zeta_{\max} = 10$. The clearest distinction between the two cases is that locations for which $|\zeta| = \zeta_{\max} = 10$ have relatively small wind speeds of less than $2\ \mathrm{m\,s^{-1}}$. Such conditions are most frequent around the Equator, especially across the Indian Ocean, as shown in Fig. 13.

5 Climatological impact on E3SM simulations

We perform a pair of 10-year simulations — CTRL and SENS described in Sect. 2.5 — to investigate the sensitivity of E3SM to the proposed changes in Alg. 3. For SENS, a tolerance of $\texttt{tol} = 10^{-4}$ is used for the stopping criterion with a maximum permissible number of iterations $\texttt{maxiter} = 2 \times 10^6$; the value of $\texttt{maxiter}$ is arbitrarily chosen to be significantly larger than expected to reach the specified tolerance. A C^0 regularization is used to enforce continuity of the exchange coefficient $\widehat{C}_{\mathrm{HN}}$ with $\varepsilon_{\mathrm{reg}} = 0.1$. A damping value of $\alpha = 0.016$ is employed in the iteration. Lastly, an initial stability limiting parameter of $\zeta_{\max} = 200$ is used with an increment of $\zeta_{\mathrm{incr}} = 0.25$ in the adaptive limiting process.

When analyzing the simulation results, one must distinguish impacts of the regularization and the revisions in the numerical algorithm from noise caused by natural variability and other sources of uncertainty in the model. To determine whether differences in the 10-year mean fluxes are statistically significant, a one-sample Student's t-test is performed using monthly mean output data. Since the data are serially correlated, we utilize a revised t-test in which the t statistic is scaled by an ef-

https://doi.org/10.5194/egusphere-2025-5430
Preprint. Discussion started: 21 January 2026

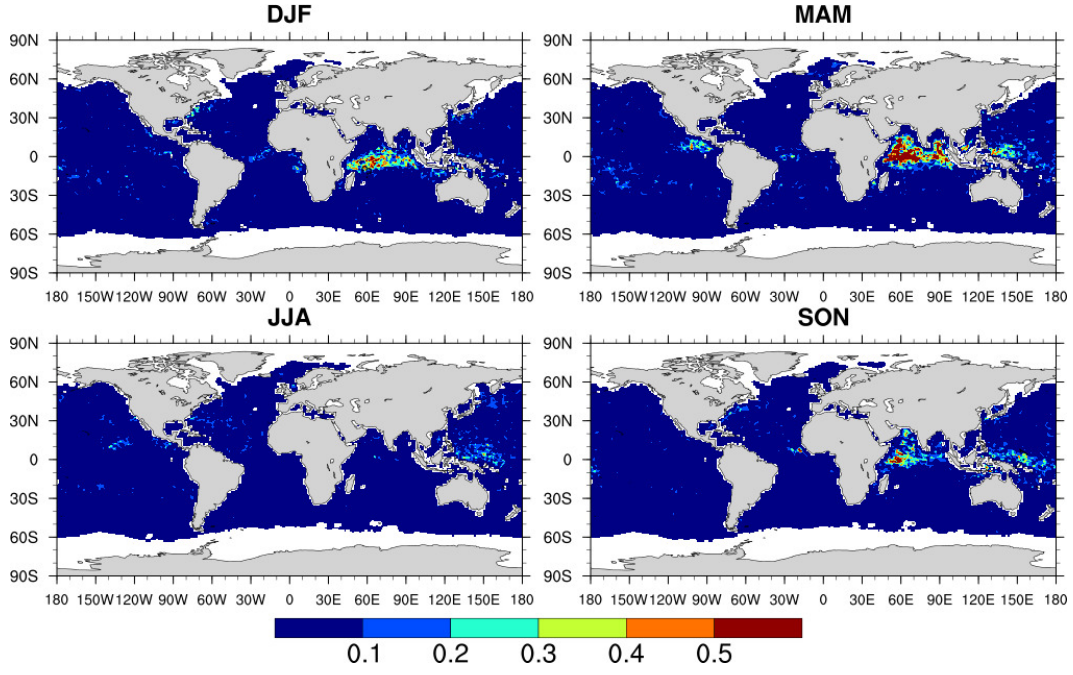

Figure 13. Percentage of days for which $|\tilde{\zeta}| = \zeta_{\max} = 10$ in ten years of daily instantaneous output from the CTRL simulation. The condition $|\tilde{\zeta}| = \zeta_{\max} = 10$ indicates that the surface fluxes lie on the manifold of solutions to (C3) which would vary with $\zeta_{\max}$. Different panels correspond to different seasons. Gray shading indicates land, and white areas are sea ice. Further details can be found in Sect. 4.5.

fective sample size (Zwiers and von Storch, 1995). A significance level of 0.05 is utilized to determine when the mean of the differences is likely to be non-zero.

The largest effects on turbulent fluxes occur in DJF (Fig. 14) and JJA (Fig. 15), while the effects in other months are substantially smaller. Statistically significant latent heat flux differences exceeding 10 $\mathrm{W\,m^{-2}}$ in magnitude and sensible heat flux differences exceeding 6 $\mathrm{W\,m^{-2}}$ in magnitude can be found in several regions, mainly over the oceans of the winter hemisphere including off of the East Asian coast, over the Gulf of Alaska, and over the Labrador Sea in DJF and over the Southern Ocean in JJA. Smaller but still statistically significant differences in latent heat fluxes are found in tropical and subtropical areas. The changes in atmospheric circulation, temperature, and humidity are small in terms of 10-year averages, but we note that in the future, it will be useful to performed fully coupled Earth system simulations to assess whether larger impacts will be seen when the atmosphere and ocean components can interact with each other.

We also performed additional sensitivity experiments using regularization parameters larger or smaller than $\varepsilon_{\mathrm{reg}} = 0.1$. These results can be found in Appendix C, Fig. C2. Within the tested range of $\varepsilon_{\mathrm{reg}} = 0.015$ to 0.5, the overall results from E3SM, in terms of 10-year averages, are not substantially different from what is presented here in Figs. 14 and 15.

https://doi.org/10.5194/egusphere-2025-5430
Preprint. Discussion started: 21 January 2026

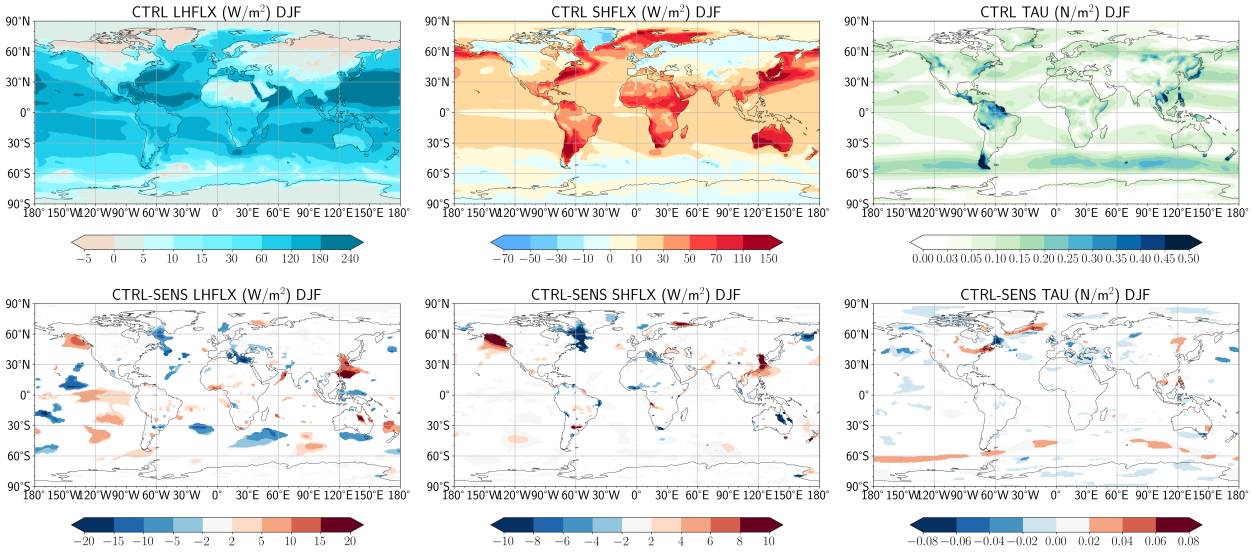

Figure 14. The 10-year mean latent heat flux (left), sensible heat flux (middle), and wind stress (right) for the months of DJF (upper row), as well as the difference between the CTRL and SENS simulations (bottom row) in which statistically insignificant differences are masked out in white.

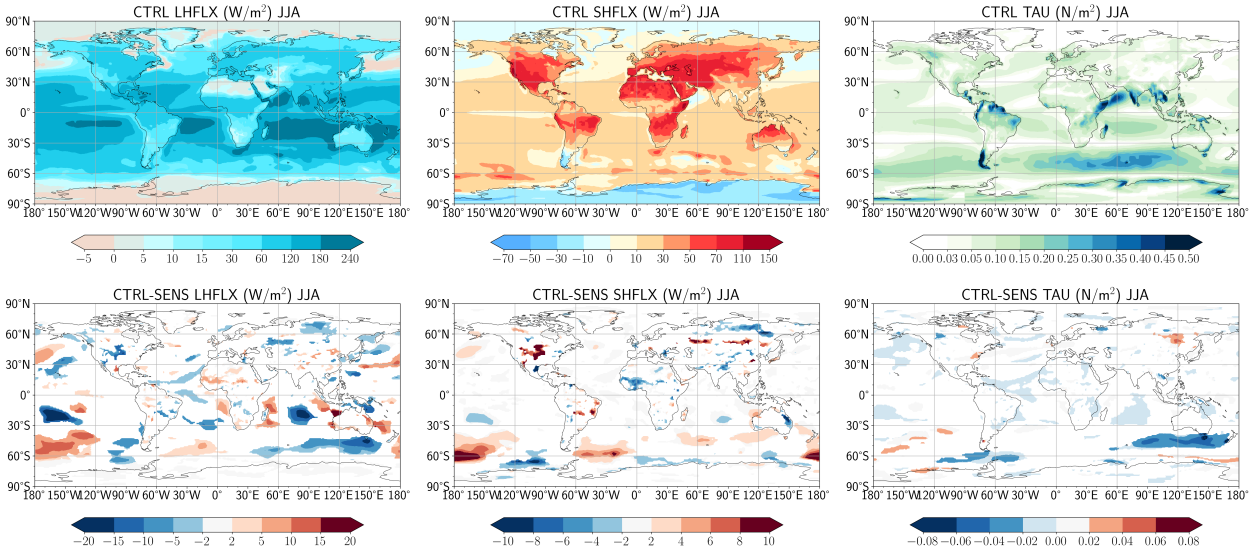

Figure 15. Same as Fig. 14 except for the months of JJA.

https://doi.org/10.5194/egusphere-2025-5430
Preprint. Discussion started: 21 January 2026

Table 1. Summary of well-posedness findings in the turbulent flux parameterization in E3SMv2 based on Large and Pond (1981) and Large and Pond (1982).

	Well-posedness issues	
Issue	**Solution non-existence**	**Solution non-uniqueness**
Cause	Discontinuous neutral heat exchange coefficient $\widehat{C}_{\mathrm{HN}}$: $\widehat{C}_{\mathrm{HN}}(\zeta) = \begin{cases} 0.0327, & \zeta < 0 \text{ (unstable)} \\ 0.0180, & \zeta \geqslant 0 \text{ (stable).} \end{cases}$ Under certain conditions, the discontinuity in $\widehat{C}_{\mathrm{HN}}$ causes the system $\boldsymbol{x} = \boldsymbol{f}(\boldsymbol{x};\boldsymbol{\xi})$ to have no solutions, i.e. the curves $\boldsymbol{x}$ and $\boldsymbol{f}(\boldsymbol{x};\boldsymbol{\xi})$ do not intersect.	*Ad hoc* Obukhov length limiter: $\tilde{\zeta} = \min(\lvert\zeta\rvert, \zeta_{\mathrm{max}}) \cdot \mathrm{sgn}(\zeta).$ Under certain conditions, when iteration "rides" the limiting value ζ_{max}, the curves $\boldsymbol{x}$ and $\boldsymbol{f}(\boldsymbol{x};\boldsymbol{\xi})$ may have two intersections.
Primary diagnostic	Oscillatory iteration which can be tracked with proper residual computation after each iteration.	Obukhov stability parameter equal to limiting value ζ_{max}, i.e. $\lvert\tilde{\zeta}\rvert = \zeta_{\mathrm{max}}$. Can be tracked by checking magnitude of $\tilde{\zeta}$ of numerical solution.
Associated meteorological conditions	Slightly stable atmospheric stratification ($0\ \mathrm{K} \lesssim \Delta\theta \lesssim 0.7\ \mathrm{K}$) occurring mostly in mid-latitude oceans and Arabian Sea	Very low wind speed ($0\ \mathrm{m/s} \lesssim U \lesssim 2\ \mathrm{m/s}$) occurring mostly in equatorial regions.
Remedy	Regularization of C_{HN} along with proper convergence testing after each iteration and throwing error if residual does not decrease.	Adaptive stability limiter which searches values of ζ_{max} until one is found which produces a solution with $\lvert\tilde{\zeta}\rvert \neq \zeta_{\mathrm{max}}$.

6 Conclusions

In this study, we have analyzed the solvability of the underlying equations of an ocean–atmosphere turbulent flux parameterization that is based on measurements discussed in Large and Pond (1981) and Large and Pond (1982) and is used by a number of ESMs, e.g., E3SM, CESM, TaiESM, NorESM, CMCC-ESM2, and RASM. Our analysis has shown that there are certain meteorological conditions, mostly encountered over the mid-latitude oceans under stable conditions, for which the turbulent flux algorithm implemented in E3SMv2 is unable to converge to a solution. This non-convergence manifests as oscillations of the scaling parameter iterates and results in a rather large residual error ($> 50\%$ on average). The likely causal factor of non-convergence is lack of solution existence in the underlying continuum equations. Moreover, we have shown that this turbulent flux algorithm does not always yield unique surface fluxes and the use of an *ad hoc* limiter on the Monin-Obukhov length has

https://doi.org/10.5194/egusphere-2025-5430
Preprint. Discussion started: 21 January 2026

a strong influence on the number of solutions. Meteorological conditions that produce non-unique solutions are found mostly in regions with low wind speed near the Equator.

We have introduced two modifications to the Large and Pond parameterization in order to enforce both existence and uniqueness of the computed surface fluxes. These modifications include (i) regularization of the discontinuous neutral exchange coefficient for heat, which resolves issues with oscillating surface fluxes corresponding to large residual errors, and (ii) adaptive selection of the limiter on the Monin-Obukhov to eliminate unintended solutions when the numerical solutions are not unique. Our analysis also points to the need to exercise caution when applying turbulent flux algorithms globally under conditions for which the underlying assumptions of the parameterization are violated. For instance, in the extreme stability limit as $\zeta \to +\infty$, the assumptions of Monin-Obukhov Similarity Theory are violated, suggesting that the Large and Pond formulation (or any parameterization based on Monin-Obukhov Similarity Theory) should not be utilized under these conditions. A summary of these issues and their remedies is provided in Table. 1.

Sensitivity of E3SMv2's mean climate to these issues of well-posedness was investigated by comparing 10-year simulations using the default formulation and algorithm (see Eq. 14, Appendix A, and Alg. 1) as well as the regularized formulation and revised algorithm (Sect. 3.3, Appendix C, and Alg. 3). The modifications lead to statistically significant differences in the 10-year mean latent and sensible heat fluxes compared to those of the default model, exceeding 10 $\mathrm{W\,m^{-2}}$ and 6 $\mathrm{W\,m^{-2}}$ in magnitudes, respectively, in various regions.

While the impacts of the revised flux algorithm on the simulated 10-year mean atmospheric circulation, temperature, and humidity are relatively small, it will be worth performing fully coupled Earth system simulations in the future to assess whether there will be larger impacts when the atmosphere and ocean components of E3SM can interact with each other. In addition, the analysis in this study demonstrates a strategy for future investigations of other ocean–atmosphere flux parameterization options in E3SM, such as the Coupled Ocean–Atmosphere Response Experiment (COARE, Fairall et al., 2003) and the University of Arizona (UA, Zeng et al., 1998) parameterizations. Furthermore, turbulent flux algorithms over sea ice and land share many similarities with the ocean–atmosphere algorithms since they too are based on MOST. They may also include discontinuous exchange coefficients in certain scenarios as well as *ad hoc* use of stability limiters as seen here in the ocean–atmosphere algorithm, which will be subjects of future research.

Beyond the topic of turbulent flux parameterizations at the Earth's surface, it is worth noting that many parameterization codes include discontinuities to distinguish between regimes, and employ limiters to avoid singularities or constrain values to physically plausible ranges. Model developers who focus primarily on the simulated physics may not always be aware that these discontinuities and limiters can significantly influence simulation outcomes, or that in mathematics and computational science, well-established techniques and concepts exist to address the underlying needs for such constructs, for instance polynomial regularization and bifurcation analysis in this paper. Some of these methods are straightforward to implement and need not incur prohibitive computational costs, as demonstrated in this study. Raising awareness of well-posedness issues in parameterizations—and of the computational techniques available to address them—is therefore a key contribution of this paper, perhaps as important as the specific improvements made to the ocean–atmosphere turbulent flux parameterization in E3SMv2.

https://doi.org/10.5194/egusphere-2025-5430
Preprint. Discussion started: 21 January 2026

Appendix A: Ocean–atmosphere turbulent flux parameterization in E3SMv2

In this section, we first clarify the expression of the exchange coefficients $C_{(\mathrm{D,H,E})}$ (Sect. A1) and then describe their adjustment to measurement height and stability which is utilized in the E3SMv2 code (Sect. A2).

A1 Exchange coefficients

The parameterization used in E3SMv2 is based on the work of Large and Pond (1981) and Large and Pond (1982) which provide expressions for C_D, C_H and C_E in terms of neutral exchange coefficients C_DN, C_HN, C_EN (see Eq. (15) in Large and Pond (1981) and Eq. (10) in Large and Pond (1982)). These expressions are as follows:

$$C_\mathrm{D} = \frac{C_\mathrm{DN}\left(u_\mathrm{10N}\right)}{\left(1+\frac{\sqrt{C_\mathrm{DN}\left(u_\mathrm{10N}\right)}}{\kappa}\left[\ln\left(\frac{z}{z_\mathrm{ref}}\right)-\psi_\mathrm{m}(\zeta)\right]\right)^2}, \tag{A1}$$

$$C_\mathrm{H} = \frac{C_\mathrm{HN}\left(u_\mathrm{10N},\zeta\right)\sqrt{\frac{C_\mathrm{D}}{C_\mathrm{DN}\left(u_\mathrm{10N}\right)}}}{\left(1+\frac{C_\mathrm{HN}\left(u_\mathrm{10N},\zeta\right)}{\kappa\sqrt{C_\mathrm{DN}\left(u_\mathrm{10N}\right)}}\left[\ln\left(\frac{z}{z_\mathrm{ref}}\right)-\psi_\mathrm{h}(\zeta)\right]\right)}, \tag{A2}$$

$$C_\mathrm{E} = \frac{C_\mathrm{EN}(u_\mathrm{10N})\sqrt{\frac{C_\mathrm{D}}{C_\mathrm{DN}\left(u_\mathrm{10N}\right)}}}{\left(1+\frac{C_\mathrm{EN}\left(u_\mathrm{10N}\right)}{\kappa\sqrt{C_\mathrm{DN}\left(u_\mathrm{10N}\right)}}\left[\ln\left(\frac{z}{z_\mathrm{ref}}\right)-\psi_\mathrm{q}(\zeta)\right]\right)}. \tag{A3}$$

Here, $z_\mathrm{ref} = 10\ \mathrm{m}$ is the reference height. The dimensionless stability functions ψ_m, ψ_h, and ψ_q are defined in terms of the Obukhov stability parameter ζ and are as follows(Large, 2006, Eq. 20):

$$\psi_\mathrm{m}(\zeta) = \begin{cases} 2\ln\left(\frac{1+\chi(\zeta)}{2}\right)+\ln\left(\frac{1+\chi(\zeta)^2}{2}\right)-2\tan^{-1}\chi(\zeta)+\frac{\pi}{2}, & \zeta<0 \\ -5\zeta, & \zeta\geqslant 0, \end{cases} \tag{A4}$$

$$\psi_\mathrm{h}(\zeta) = \psi_\mathrm{q}(\zeta) = \begin{cases} \ln\left(\frac{1+\chi(\zeta)^2}{2}\right), & \zeta<0 \\ -5\zeta, & \zeta\geqslant 0, \end{cases} \tag{A5}$$

where $\chi(\zeta) = |1-16\zeta|^{1/4}$ (see Eq. (20) in Large (2006) but note that the parentheses therein need to be replaced by an absolute value sign). The stability functions ψ_m, ψ_h, and ψ_q are continuous at $\zeta = 0$ despite their piecewise definitions. The neutral exchange coefficients are defined as follows.

- For momentum (Large, 2006, Eq. (34)),

$$C_\mathrm{DN}(u_\mathrm{10N}) = \frac{0.0027}{u_\mathrm{10N}} + 0.000142 + 0.0000764\,u_\mathrm{10N}. \tag{A6}$$

https://doi.org/10.5194/egusphere-2025-5430
Preprint. Discussion started: 21 January 2026

– For heat (Large and Pond, 1982, Eq. (23)),

$$C_{\mathrm{HN}}(u_{10\mathrm{N}},\zeta) = \begin{cases} \sqrt{C_{\mathrm{DN}}(u_{10\mathrm{N}})}\cdot 0.0327, & \text{if } \zeta < 0 \\ \sqrt{C_{\mathrm{DN}}(u_{10\mathrm{N}})}\cdot 0.018, & \text{if } \zeta \geqslant 0\,. \end{cases} \tag{A7}$$

– For moisture (Large and Pond, 1982, Eq. (24))),

$$C_{\mathrm{EN}}(u_{10\mathrm{N}}) = \sqrt{C_{\mathrm{DN}}(u_{10\mathrm{N}})}\cdot 0.0346\,. \tag{A8}$$

We see from Eq. (A1)-(A3) that the exchange coefficients are functions of $u_{10\mathrm{N}}$, ζ, and z (represented by the bulk meteorological variables $\boldsymbol{\xi}$), i.e.,

$$C_{(\mathrm{D,H,E})} = C_{(\mathrm{D,H,E})}\left(u_{10\mathrm{N}},\zeta;\boldsymbol{\xi}\right). \tag{A9}$$

A2 Nonlinear equation solved in E3SMv2

Neglecting wind gustiness (i.e., assuming $S = U$) and combining Eqs. (4)-(6) with Eqs. (8)-(10) to eliminate the eddy covariances, we obtain

$$\frac{u_*^2}{U^2} = C_{\mathrm{D}}\,, \quad \frac{\theta_*}{\Delta\theta} = C_{\mathrm{H}}\frac{U}{u_*}\,, \quad \frac{q_*}{\Delta q} = C_{\mathrm{E}}\frac{U}{u_*}\,. \tag{A10}$$

We introduce the new set of symbols $\widehat{C}_{(\mathrm{D,H,E})}$ to denote the adjusted exchange coefficients which are defined by

$$\widehat{C}_{\mathrm{D}} := \frac{u_*}{U} = \sqrt{C_{\mathrm{D}}}, \quad \widehat{C}_{\mathrm{H}} := C_{\mathrm{H}}\frac{u_*}{U} = \frac{C_{\mathrm{H}}}{\sqrt{C_{\mathrm{D}}}}, \quad \widehat{C}_{\mathrm{E}} := C_{\mathrm{E}}\frac{u_*}{U} = \frac{C_{\mathrm{E}}}{\sqrt{C_{\mathrm{D}}}}, \tag{A11}$$

and write Eq. (A10) as

$$u_* = \widehat{C}_{\mathrm{D}}\,U\,, \quad \theta_* = \widehat{C}_H\Delta\theta\,, \quad q_* = \widehat{C}_{\mathrm{E}}\Delta q\,. \tag{A12}$$

The definitions of $\widehat{C}_{(\mathrm{D,H,E})}$ in Eq. (A11) may be expanded using Eqs. (A1)-(A3) to obtain

$$\begin{aligned} \widehat{C}_D &= \frac{\sqrt{C_{\mathrm{DN}}(u_{10\mathrm{N}})}}{1+\frac{\sqrt{C_{\mathrm{DN}}(u_{10\mathrm{N}})}}{\kappa}\left[\ln\left(\frac{z}{z_{\mathrm{ref}}}\right)-\psi_{\mathrm{m}}\left(\zeta\right)\right]}\,, \\ \widehat{C}_H &= \frac{\widehat{C}_{\mathrm{HN}}(\zeta)}{1+\frac{\widehat{C}_{\mathrm{HN}}(\zeta)}{\kappa}\left[\ln\left(\frac{z}{z_{\mathrm{ref}}}\right)-\psi_{\mathrm{h}}\left(\zeta\right)\right]}\,, \\ \widehat{C}_E &= \frac{\widehat{C}_{\mathrm{EN}}}{1+\frac{\widehat{C}_{\mathrm{EN}}}{\kappa}\left[\ln\left(\frac{z}{z_{\mathrm{ref}}}\right)-\psi_{\mathrm{q}}\left(\zeta\right)\right]}\,, \end{aligned} \tag{A13}$$

https://doi.org/10.5194/egusphere-2025-5430
Preprint. Discussion started: 21 January 2026

where the adjusted neutral exchange coefficients $\widehat{C}_{\mathrm{HN}}$ and $\widehat{C}_{\mathrm{EN}}$ no longer depend on the neutral 10 m wind speed and are given by

$$\widehat{C}_{\mathrm{HN}}(\zeta) = \frac{C_{\mathrm{HN}}(u_{10\mathrm{N}}, \zeta)}{\sqrt{C_{\mathrm{DN}}(u_{10\mathrm{N}})}} = \begin{cases} 0.0327, & \zeta < 0 \\ 0.018, & \zeta \geqslant 0 \end{cases}, \qquad \widehat{C}_{\mathrm{EN}} = \frac{C_{\mathrm{EN}}(u_{10\mathrm{N}})}{\sqrt{C_{\mathrm{DN}}(u_{10\mathrm{N}})}} = 0.0346. \tag{A14}$$

Finally, the neutral 10 m wind speed is itself a function of the friction velocity u_* and C_{DN} and is given by the nonlinear equation

$$u_{10\mathrm{N}} = \frac{u_*}{\sqrt{C_{\mathrm{DN}}(u_{10\mathrm{N}})}}. \tag{A15}$$

Eq. (A15) together with Eq. (A12) constitutes the nonlinear system of equations as implemented in E3SMv2.

Appendix B: Discontinuity and solution existence

Discontinuities in the neutral exchange coefficient C_{HN} can cause Eq. (13) to have no solutions. However, the presence of the discontinuity is not in itself a guarantee of solution non-existence. Fig. B1 shows two possible scenarios with abstract

Scenario	Example	Suspected meteorological conditions
No solution since the discontinuity in $\boldsymbol{f}_3$ coincides with θ_*.	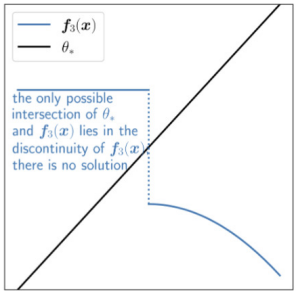	Appears to be associated with mildly stable atmospheric conditions $0 < \Delta\theta < 0.7$, see Figure 5.
Solution exists since $\boldsymbol{f}_3$ and θ_* intersect away from the discontinuity in $\boldsymbol{f}_3$.	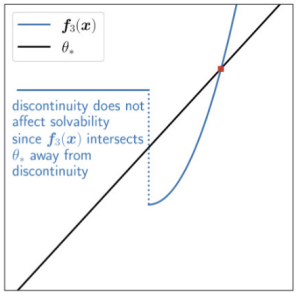	Appears to be associated with unstable atmospheric conditions as well as stable conditions with $\Delta\theta > 0.7$.

Figure B1. A graphical visualization of the existence or non-existence of a solution to the Large and Pond turbulent flux parameterization equations (13) due to the discontinuity in the neutral heat exchange coefficient $\widehat{C}_{\mathrm{HN}}$. We focus on the third equation of (15) which contains the discontinuity and may be written as $\theta_* = f_3(\boldsymbol{x})$.

https://doi.org/10.5194/egusphere-2025-5430
Preprint. Discussion started: 21 January 2026

illustrations in one dimension to demonstrate when the discontinuity causes solution non-existence. Based on offline analysis of the 10-year CTRL simulation described in Sect. 2.5, we are able to link each of the scenarios in Fig. B1 to different stability regimes in the atmosphere. In particular, it appears (see Fig. 3) that the discontinuity only causes solution non-existence under mildly stable atmospheric conditions while unstable conditions as well as stable conditions with $\Delta\theta > 0.7$ do not pose any issues to solution existence.

Appendix C: Regularization of the neutral heat exchange coefficient

The discontinuous neutral heat exchange coefficient $\widehat{C}_{\mathrm{HN}}$ is replaced by the regularized coefficient

$$\widehat{C}^{(k)}_{\mathrm{HN},\varepsilon_{\mathrm{reg}}}(\zeta) := \begin{cases} 0.0327, & \zeta \leqslant -\varepsilon_{\mathrm{reg}} \\ p^{(k)}_{\varepsilon_{\mathrm{reg}}}(\zeta), & -\varepsilon_{\mathrm{reg}} < \zeta \leqslant \varepsilon_{\mathrm{reg}} \\ 0.018, & \zeta > \varepsilon_{\mathrm{reg}} \end{cases}.$$

The polynomial $p^{(k)}_{\varepsilon_{\mathrm{reg}}}$ is given by

$$p^{(k)}_{\varepsilon_{\mathrm{reg}}}(\zeta) := \sum_{j=0}^{2k+1} a_j \zeta^j, \quad \varepsilon_{\mathrm{reg}} > 0, \tag{C1}$$

where the coefficients, a_j, are obtained by enforcing the continuity conditions

$$p^{(k)}_{\varepsilon_{\mathrm{reg}}}(-\varepsilon_{\mathrm{reg}}) = 0.0327, \quad p^{(k)}_{\varepsilon_{\mathrm{reg}}}(\varepsilon_{\mathrm{reg}}) = 0.018, \quad \left.\frac{d^j p_{k,\varepsilon_{\mathrm{reg}}}}{d\zeta^j}\right|_{\zeta=\pm\varepsilon_{\mathrm{reg}}} = 0, \quad 1 \leqslant j \leqslant k,$$

which amounts to solving a system of $2k+2$ linear equations.

For the fixed-point and nonlinear Gauss-Seidel iterations employed by E3SM, enforcing C^0 continuity — i.e. continuity of just $\widehat{C}^{(k)}_{\mathrm{HN},\varepsilon_{\mathrm{reg}}}$ — is enough to allow these methods to converge. However, we have provided the polynomial regularization for enforcing general continuity of up to order k derivatives $\widehat{C}^{(k)}_{\mathrm{HN},\varepsilon_{\mathrm{reg}}}$ since higher-order iterative methods such as Newton's method require C^1 or even stronger continuity of the right-hand side function $\boldsymbol{f}$. For completeness, we state the C^0 and C^1 polynomials below:

$$p^{(0)}_{\varepsilon_{\mathrm{reg}}}(\zeta) = 0.02535 - \frac{0.00735}{\varepsilon_{\mathrm{reg}}}\zeta$$

$$p^{(1)}_{\varepsilon_{\mathrm{reg}}}(\zeta) = 0.02535 - \frac{0.011025}{\varepsilon_{\mathrm{reg}}}\zeta + \frac{0.003675}{\varepsilon^3_{\mathrm{reg}}}\zeta^3.$$

With the regularized neutral heat exchange coefficient $\widehat{C}^{(k)}_{\mathrm{HN},\varepsilon_{\mathrm{reg}}}$, we may define a corresponding regularized heat exchange coefficient $\widehat{C}^{(k)}_{\mathrm{H},\varepsilon_{\mathrm{reg}}}$:

$$\widehat{C}^{(k)}_{\mathrm{H},\varepsilon_{\mathrm{reg}}}(u_{10\mathrm{N}},\zeta;\boldsymbol{\xi}) := \frac{\widehat{C}^{(k)}_{\mathrm{HN},\varepsilon_{\mathrm{reg}}}(\zeta)}{1 + \frac{\widehat{C}^{(k)}_{\mathrm{HN},\varepsilon_{\mathrm{reg}}}(\zeta)}{\kappa}\left[\left(\frac{z}{z_{\mathrm{ref}}}\right) - \psi_{\mathrm{h}}(\zeta)\right]} \tag{C2}$$

https://doi.org/10.5194/egusphere-2025-5430
Preprint. Discussion started: 21 January 2026

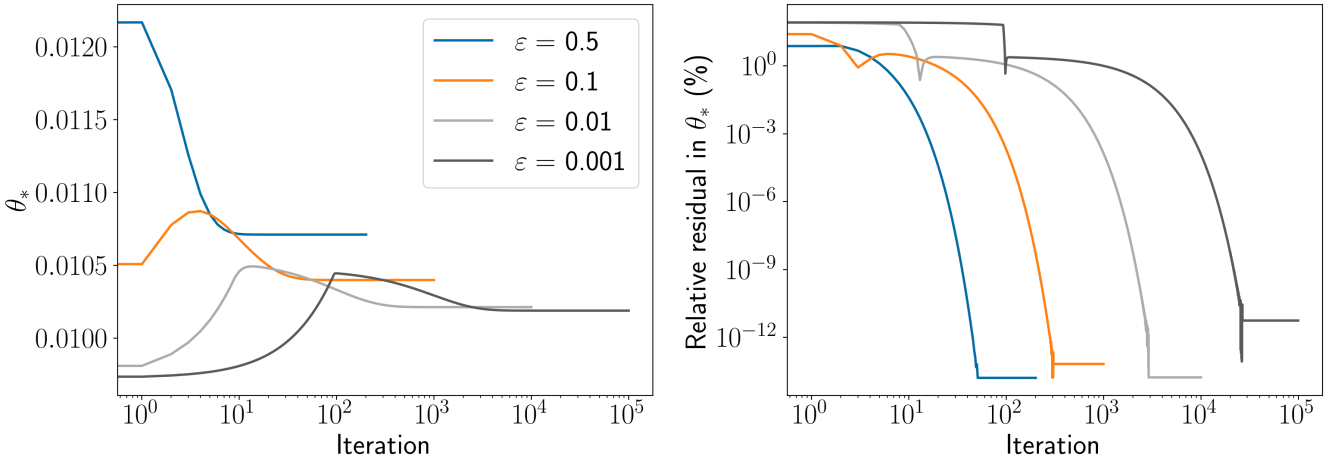

Figure C1. The iterate $(\theta_*)_n$ and its relative residual when approximating the solution of the regularized turbulent flux parameterization (C3) with conditions described by (20). The value of the regularization parameter is chosen from $\varepsilon_{\text{reg}} \in \{0.5, 0.1, 0.01, 0.001\}$ with damping parameter $\alpha = \varepsilon_{\text{reg}}$.

Finally, the regularized turbulent flux parameterization based on the Large and Pond (1982) parameterization is given by

$$\begin{cases} u_* = \widehat{C}_{\text{D}}\Big(u_{10\text{N}}, \zeta(u_*, \theta_*, q_*); \boldsymbol{\xi}\Big) \cdot U\,, \\ u_{10\text{N}} = \dfrac{\widehat{C}_{\text{D}}\Big(u_{10\text{N}}, \zeta(u_*, \theta_*, q_*); \boldsymbol{\xi}\Big)}{\sqrt{C_{\text{DN}}(u_{10\text{N}})}} \cdot U\,, \\ \theta_* = \widehat{C}^{(k)}_{\text{H},\varepsilon_{\text{reg}}}\Big(u_{10\text{N}}, \zeta(u_*, \theta_*, q_*); \boldsymbol{\xi}\Big) \cdot \Delta\theta\,, \\ q_* = \widehat{C}_{\text{E}}\Big(u_{10\text{N}}, \zeta(u_*, \theta_*, q_*); \boldsymbol{\xi}\Big) \cdot \Delta q. \end{cases} \tag{C3}$$

The effect of the regularization parameter ε_{reg} on the convergence of iterations is shown in Fig. C1 for the meteorological conditions described by Eq. (20). As discussed in Sect. 3.3, the particular construction of the regularized neutral heat exchange coefficient (21) means that smaller values of ε_{reg} introduce sharper gradients to $\boldsymbol{f}$ which require smaller values of the damping parameter α to resolve in Alg. 2. Indeed, we observe nearly an order of magnitude increase in the number of iterations required to reach a relative residual of 10^{-12} for each order of magnitude decrease in ε_{reg}.

To determine the effect of the regularization parameter on the overall Earth system, we consider the differences between the CTRL latent and sensible heat fluxes and wind stress, which are computed using the default E3SMv2 algorithm (Alg. 1) without any modifications to address solution non-existence and non-uniqueness, and the corresponding fluxes obtained from a sequence of simulations with $\varepsilon_{\text{reg}} = 0.5, 0.1, 0.015$ and a fixed $\zeta_{\text{max}} = 200$ (Alg. 3). The CTRL and regularized turbulent fluxes are not substantially different as ε_{reg} is decreased. For this reason, we suggest taking $\varepsilon_{\text{reg}} = 0.1$ to capture the most significant changes resulting from the regularization.

https://doi.org/10.5194/egusphere-2025-5430
Preprint. Discussion started: 21 January 2026

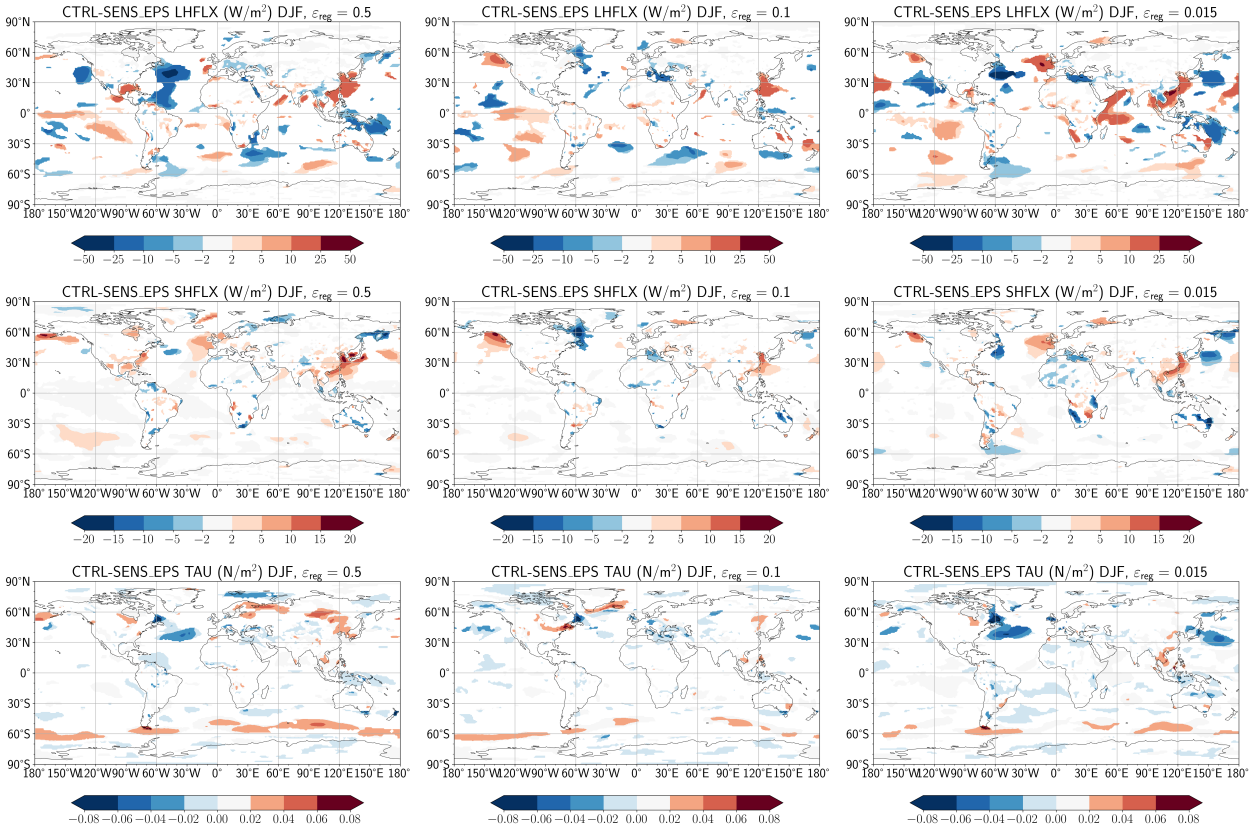

Figure C2. 10-year mean differences in latent heat flux (top row), sensible heat flux (middle row), and wind stress (bottom row) between CTRL simulation and a sequence of simulations with $\varepsilon_{\text{reg}} = 0.5, 0.1, 0.015$ (from left to right). The initial adaptive stability limiter described in Sect. 4.4 is fixed at $\zeta_{\text{max}} = 20$.

https://doi.org/10.5194/egusphere-2025-5430
Preprint. Discussion started: 21 January 2026

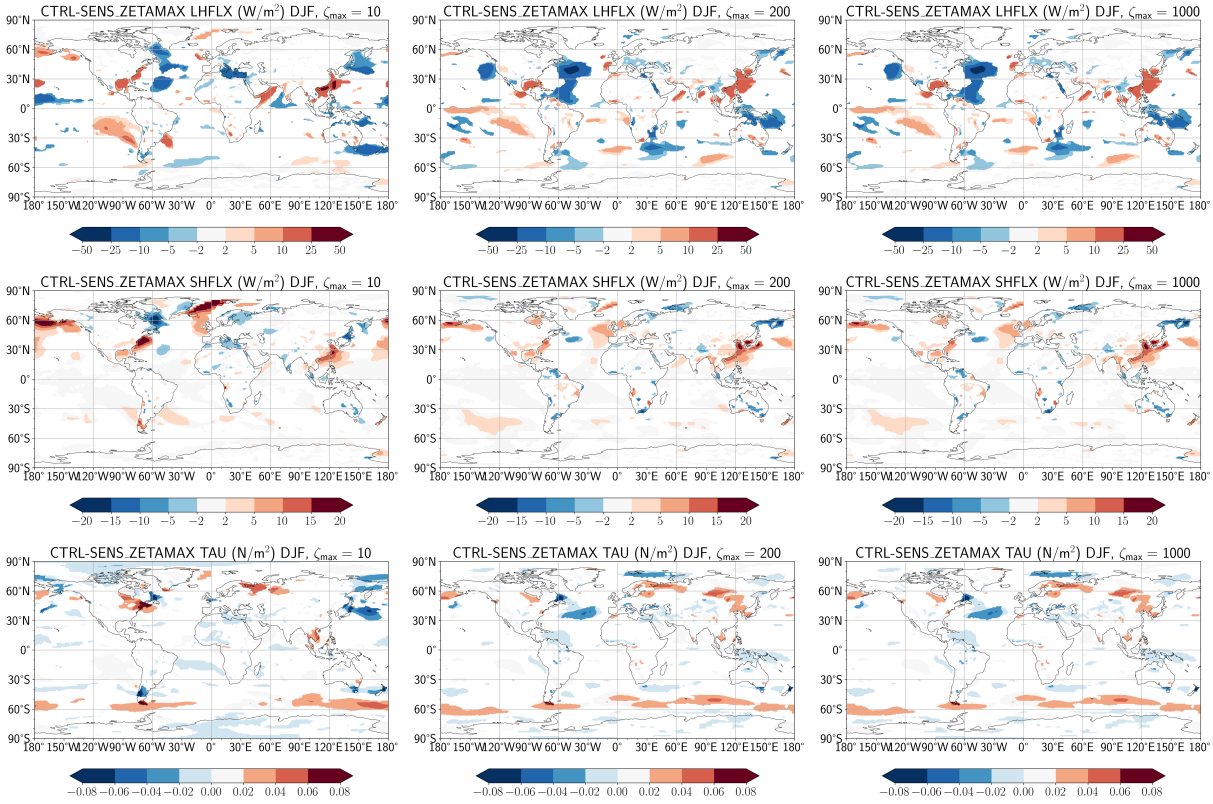

Figure D1. 10-year mean differences in latent heat flux (top row), sensible heat flux (middle row), and wind stress (bottom row) between CTRL simulation and a sequence of simulations with $\zeta_{\max} = 20, 200, 1000$ (from left to right). The regularization parameter ε_{reg} is fixed at 0.5.

Appendix D: Selection of adaptive limiter parameter

The adaptive limiter described in Sect. 4.4 requires one to select an initial value of $\zeta_{\max}$, which is then decreased if no suitable solution is found that satisfies $|\zeta| \neq \zeta_{\max}$. In certain scenarios, for instance the second panel of Fig. 10, the initial value of $\zeta_{\max}$ must be sufficiently large in order for the system of equations describing the ocean–atmosphere turbulent fluxes to have a solution that does not vary with $\zeta_{\max}$. If $\zeta_{\max}$ is chosen too small, the adaptive limiting algorithm may terminate without finding a solution for which $|\zeta| \neq \zeta_{\max}$. To this end, we perform a numerical experiment in which the value of the regularization parameter, ε_{reg}, is held fixed and the initial limiting parameter is varied. A reference simulation is generated with $\zeta_{\max} = 1000$ and the latent and sensible heat fluxes are compared with those from a sequence of simulations with $\zeta_{\max} = 20$ and 200 (Fig. D1). We observe that an initial limiting parameter value of $\zeta_{\max} = 200$ allows Algorithm 3 to return the same turbulent fluxes as an initial value of $\zeta_{\max} = 1000$. We thus recommend $\zeta_{\max} = 200$ in Algorithm 3.

https://doi.org/10.5194/egusphere-2025-5430
Preprint. Discussion started: 21 January 2026

Code and data availability. Simulation output data corresponding to the CTRL and SENS simulations and sensitivity runs in Appendices C and D may be found in https://doi.org/10.5281/zenodo.17498126 (Dong et al., 2025b), https://doi.org/10.5281/zenodo.17498147 (Dong et al., 2025c), and https://doi.org/10.5281/zenodo.17510833 (Dong et al., 2025d). Python scripts used to generate bifurcation diagrams, create corner plots, and analyze convergence of the turbulent flux algorithms may be found in https://doi.org/10.5281/zenodo.17511114 (Dong et al., 2025a). A fork of E3SMv2 containing the proposed changes to E3SM's ocean–atmosphere turbulent flux algorithm in Algorithm 3 may be found at the repository https://doi.org/10.5281/zenodo.18180192 (Dong, 2025).

Author contributions. XZ and CSW initiated this study. JD evaluated the Large and Pond algorithm for issues of existence and uniqueness. JD developed and implemented the regularization, damped fixed-point iteration, and adaptive stability limiter with contribution from CSW and CJV. JD performed the CTRL and SENS simulations using E3SM and processed the simulation output; MAB, XZ, and HW contributed to the analysis of the results. JD performed and analyzed offline calculations using E3SM simulation output provided by HW. JD led the writing of this paper with input from all co-authors.

Competing interests. The authors declare that they have no conflict of interest.

Acknowledgements. The authors would like to thank Sean P. Santos for helpful discussions and feedback in the writing of this manuscript; Kezhen Chong for her guidance in post-processing E3SM simulation data; Arshia Singhal for her initial investigation of the use of Anderson acceleration techniques for computing turbulent fluxes; and Sean P. Santos and Philip J. Rasch for their assistance in identifying current Earth system models that utilize the Large and Pond turbulent flux parameterization.

This research used resources of the National Energy Research Scientific Computing Center (NERSC), a U.S. Department of Energy Office of Science User Facility located at Lawrence Berkeley National Laboratory, operated under Contract No. DE-AC02-05CH11231 using NERSC award ASCR-ERCAP0028881.

This work was performed under the auspices of the U.S. Department of Energy by Lawrence Livermore National Laboratory under Contract DE-AC52-07NA27344. LLNL-JRNL-2001306-DRAFT. Pacific Northwest National Laboratory is operated for the U.S. Department of Energy by Battelle Memorial Institute under contract DE-AC06-76RLO1830.

Financial support. This material is based upon work supported by the U.S. Department of Energy, Office of Science, Office of Advanced Scientific Computing Research (ASCR), Office of Biological and Environmental Research (BER), Scientific Discovery through Advanced Computing (SciDAC) program, via an ASCR-BER partnership in Earth System Model Development; and by the U.S. Department of Energy, Office of Science, ASCR via the Frameworks, Algorithms, and Software Technologies for Mathematics SciDAC Institute program.

https://doi.org/10.5194/egusphere-2025-5430
Preprint. Discussion started: 21 January 2026

References

Anderson, D. G.: Iterative procedures for nonlinear integral equations, Journal of the ACM (JACM), 12, 547–560, 1965.

Bentsen, M., Bethke, I., Debernard, J. B., Iversen, T., Kirkevåg, A., Seland, Ø., Drange, H., Roelandt, C., Seierstad, I. A., Hoose, C., and Kristjánsson, J. E.: The Norwegian Earth System Model, NorESM1-M – Part 1: Description and basic evaluation of the physical climate, Geoscientific Model Development, 6, 687–720, https://doi.org/10.5194/gmd-6-687-2013, 2013.

Brunke, M. A., Zeng, X., and Anderson, S.: Uncertainties in sea surface turbulent flux algorithms and data sets, Journal of Geophysical Research: Oceans, 107, 5–1–5–21, https://doi.org/10.1029/2001JC000992, 2002.

Brunke, M. A., Fairall, C. W., Zeng, X., Eymard, L., and Curry, J. A.: Which Bulk Aerodynamic Algorithms are Least Problematic in Computing Ocean Surface Turbulent Fluxes?, Journal of Climate, 16, 619 – 635, https://doi.org/10.1175/1520-0442(2003)016<0619:WBAAAL>2.0.CO;2, 2003.

Cassano, J. J., DuVivier, A., Roberts, A., Abel, M. R., Seefeldt, M., Brunke, M., Craig, A., Fisel, B., Gutowski, W., Hamman, J., Higgins, M., Maslowski, W., Nijssen, B., Osinski, R., and Zeng, X.: Development of the Regional Arctic System Model (RASM): Near-Surface Atmospheric Climate Sensitivity, Journal of Climate, 30, 5729 – 5753, https://doi.org/10.1175/JCLI-D-15-0775.1, 2017.

Chang, H.-R. and Grossman, R. L.: Evaluation of bulk surface flux algorithms for light wind conditions using data from the Coupled Ocean-Atmosphere Response Experiment (COARE), Quarterly Journal of the Royal Meteorological Society, 125, 1551–1588, https://doi.org/https://doi.org/10.1002/qj.49712555705, 1999.

Chow, S.-N. and Hale, J. K.: Methods of bifurcation theory, vol. 251, Springer Science & Business Media, 2012.

Danabasoglu, G., Lamarque, J.-F., Bacmeister, J., Bailey, D. A., DuVivier, A. K., Edwards, J., Emmons, L. K., Fasullo, J., Garcia, R., Gettelman, A., Hannay, C., Holland, M. M., Large, W. G., Lauritzen, P. H., Lawrence, D. M., Lenaerts, J. T. M., Lindsay, K., Lipscomb, W. H., Mills, M. J., Neale, R., Oleson, K. W., Otto-Bliesner, B., Phillips, A. S., Sacks, W., Tilmes, S., van Kampenhout, L., Vertenstein, M., Bertini, A., Dennis, J., Deser, C., Fischer, C., Fox-Kemper, B., Kay, J. E., Kinnison, D., Kushner, P. J., Larson, V. E., Long, M. C., Mickelson, S., Moore, J. K., Nienhouse, E., Polvani, L., Rasch, P. J., and Strand, W. G.: The Community Earth System Model Version 2 (CESM2), Journal of Advances in Modeling Earth Systems, 12, e2019MS001 916, https://doi.org/https://doi.org/10.1029/2019MS001916, e2019MS001916 2019MS001916, 2020.

Dong, J.: PAESCAL-SciDAC5/E3SM-fork: Ocean atmosphere turbulent flux revisions (ocean_atm_flux_paper), https://doi.org/10.5281/zenodo.18180192, 2025.

Dong, J., Brunke, M. A., Zeng, X., Woodward, C. S., Vogl, C. J., and Wan, H.: E3SMv2 offline analysis of ocean-atmosphere turbulent flux parameterization, https://doi.org/10.5281/zenodo.17511114, 2025a.

Dong, J., Brunke, M. A., Zeng, X., Woodward, C. S., Vogl, C. J., and Wan, H.: E3SMv2 climatology and time series output for analysis of ocean-atmosphere turbulent flux parameterization (pt 1), https://doi.org/10.5281/zenodo.17498126, 2025b.

Dong, J., Brunke, M. A., Zeng, X., Woodward, C. S., Vogl, C. J., and Wan, H.: E3SMv2 climatology and time series output for analysis of ocean-atmosphere turbulent flux parameterization (pt 2), https://doi.org/10.5281/zenodo.17498147, 2025c.

Dong, J., Brunke, M. A., Zeng, X., Woodward, C. S., Vogl, C. J., and Wan, H.: E3SMv2 climatology and time series output for analysis of ocean-atmosphere turbulent flux parameterization (pt 3), https://doi.org/10.5281/zenodo.17510833, 2025d.

Fairall, C. W., Bradley, E. F., Hare, J. E., Grachev, A. A., and Edson, J. B.: Bulk Parameterization of Air–Sea Fluxes: Updates and Verification for the COARE Algorithm, Journal of Climate, 16, 571 – 591, https://doi.org/10.1175/1520-0442(2003)016<0571:BPOASF>2.0.CO;2, 2003.

https://doi.org/10.5194/egusphere-2025-5430
Preprint. Discussion started: 21 January 2026

Gardner, D. J., Guerra, J. E., Hamon, F. P., Reynolds, D. R., Ullrich, P. A., and Woodward, C. S.: Implicit–explicit (IMEX) Runge–Kutta methods for non-hydrostatic atmospheric models, Geoscientific Model Development, 11, 1497–1515, https://doi.org/10.5194/gmd-11-1497-2018, 2018.

Gardner, D. J., Reynolds, D. R., Woodward, C. S., and Balos, C. J.: Enabling new flexibility in the SUNDIALS suite of nonlinear and differential/algebraic equation solvers, ACM Transactions on Mathematical Software (TOMS), 48, 1–24, https://doi.org/https://doi.org/10.1145/353980, 2022.

Golaz, J.-C., Van Roekel, L. P., Zheng, X., Roberts, A. F., Wolfe, J. D., Lin, W., Bradley, A. M., Tang, Q., Maltrud, M. E., Forsyth, R. M., Zhang, C., Zhou, T., Zhang, K., Zender, C. S., Wu, M., Wang, H., Turner, A. K., Singh, B., Richter, J. H., Qin, Y., Petersen, M. R., Mametjanov, A., Ma, P.-L., Larson, V. E., Krishna, J., Keen, N. D., Jeffery, N., Hunke, E. C., Hannah, W. M., Guba, O., Griffin, B. M., Feng, Y., Engwirda, D., Di Vittorio, A. V., Dang, C., Conlon, L. M., Chen, C.-C.-J., Brunke, M. A., Bisht, G., Benedict, J. J., Asay-Davis, X. S., Zhang, Y., Zhang, M., Zeng, X., Xie, S., Wolfram, P. J., Vo, T., Veneziani, M., Tesfa, T. K., Sreepathi, S., Salinger, A. G., Reeves Eyre, J. E. J., Prather, M. J., Mahajan, S., Li, Q., Jones, P. W., Jacob, R. L., Huebler, G. W., Huang, X., Hillman, B. R., Harrop, B. E., Foucar, J. G., Fang, Y., Comeau, D. S., Caldwell, P. M., Bartoletti, T., Balaguru, K., Taylor, M. A., McCoy, R. B., Leung, L. R., and Bader, D. C.: The DOE E3SM Model Version 2: Overview of the Physical Model and Initial Model Evaluation, Journal of Advances in Modeling Earth Systems, 14, e2022MS003 156, https://doi.org/https://doi.org/10.1029/2022MS003156, e2022MS003156 2022MS003156, 2022.

Hannah, W. M., Bradley, A. M., Guba, O., Tang, Q., Golaz, J.-C., and Wolfe, J.: Separating Physics and Dynamics Grids for Improved Computational Efficiency in Spectral Element Earth System Models, Journal of Advances in Modeling Earth Systems, 13, e2020MS002 419, https://doi.org/https://doi.org/10.1029/2020MS002419, e2020MS002419 2020MS002419, 2021.

Harrop, B. E., Ma, P.-L., Rasch, P. J., Neale, R. B., and Hannay, C.: The Role of Convective Gustiness in Reducing Seasonal Precipitation Biases in the Tropical West Pacific, Journal of Advances in Modeling Earth Systems, 10, 961–970, https://doi.org/10.1002/2017MS001157, 2018.

Hindmarsh, A. C., Brown, P. N., Grant, K. E., Lee, S. L., Serban, R., Shumaker, D. E., and Woodward, C. S.: SUNDIALS: Suite of nonlinear and differential/algebraic equation solvers, ACM Transactions on Mathematical Software, 31, 363–396, https://doi.org/10.1145/1089014.1089020, 2005.

Hurrell, J. W., Holland, M. M., Gent, P. R., Ghan, S., Kay, J. E., Kushner, P. J., Lamarque, J.-F., Large, W. G., Lawrence, D., Lindsay, K., Lipscomb, W. H., Long, M. C., Mahowald, N., Marsh, D. R., Neale, R. B., Rasch, P., Vavrus, S., Vertenstein, M., Bader, D., Collins, W. D., Hack, J. J., Kiehl, J., and Marshall, S.: The Community Earth System Model: A Framework for Collaborative Research, Bulletin of the American Meteorological Society, 94, 1339 – 1360, https://doi.org/10.1175/BAMS-D-12-00121.1, 2013.

Isaacson, E. and Keller, H. B.: Analysis of numerical methods, Courier Corporation, 1994.

Kawai, H., Yoshida, K., Koshiro, T., and Yukimoto, S.: Importance of Minor-Looking Treatments in Global Climate Models, Journal of Advances in Modeling Earth Systems, 14, e2022MS003 128, https://doi.org/10.1029/2022MS003128, 2022.

Large, W. G.: Surface Fluxes for Practitioners of Global Ocean Data Assimilation, pp. 229–270, Springer Netherlands, Dordrecht, ISBN 978-1-4020-4028-3, https://doi.org/10.1007/1-4020-4028-8_9, 2006.

Large, W. G. and Caron, J. M.: Diurnal cycling of sea surface temperature, salinity, and current in the CESM coupled climate model, Journal of Geophysical Research: Oceans, 120, 3711–3729, https://doi.org/10.1002/2014JC010691, 2015.

Large, W. G. and Pond, S.: Open Ocean Momentum Flux Measurements in Moderate to Strong Winds, Journal of Physical Oceanography, 11, 324 – 336, https://doi.org/10.1175/1520-0485(1981)011<0324:OOMFMI>2.0.CO;2, 1981.

https://doi.org/10.5194/egusphere-2025-5430
Preprint. Discussion started: 21 January 2026

Large, W. G. and Pond, S.: Sensible and latent heat flux measurements over the ocean, Journal of physical Oceanography, 12, 464–482, https://doi.org/10.1175/1520-0485(1982)012<0464:SALHFM>2.0.CO;2, 1982.

Lee, W.-L., Wang, Y.-C., Shiu, C.-J., Tsai, I., Tu, C.-Y., Lan, Y.-Y., Chen, J.-P., Pan, H.-L., and Hsu, H.-H.: Taiwan Earth System Model Version 1: description and evaluation of mean state, Geoscientific Model Development, 13, 3887–3904, https://doi.org/10.5194/gmd-13-3887-2020, 2020.

Lovato, T., Peano, D., Butenschön, M., Materia, S., Iovino, D., Scoccimarro, E., Fogli, P. G., Cherchi, A., Bellucci, A., Gualdi, S., Masina, S., and Navarra, A.: CMIP6 Simulations With the CMCC Earth System Model (CMCC-ESM2), Journal of Advances in Modeling Earth Systems, 14, e2021MS002 814, https://doi.org/https://doi.org/10.1029/2021MS002814, e2021MS002814 2021MS002814, 2022.

Ma, P.-L., Harrop, B. E., Larson, V. E., Neale, R. B., Gettelman, A., Morrison, H., Wang, H., Zhang, K., Klein, S. A., Zelinka, M. D., Zhang, Y., Qian, Y., Yoon, J.-H., Jones, C. R., Huang, M., Tai, S.-L., Singh, B., Bogenschutz, P. A., Zheng, X., Lin, W., Quaas, J., Chepfer, H., Brunke, M. A., Zeng, X., Mülmenstädt, J., Hagos, S., Zhang, Z., Song, H., Liu, X., Pritchard, M. S., Wan, H., Wang, J., Tang, Q., Caldwell, P. M., Fan, J., Berg, L. K., Fast, J. D., Taylor, M. A., Golaz, J.-C., Xie, S., Rasch, P. J., and Leung, L. R.: Better calibration of cloud parameterizations and subgrid effects increases the fidelity of the E3SM Atmosphere Model version 1, Geoscientific Model Development, 15, 2881–2916, https://doi.org/10.5194/gmd-15-2881-2022, 2022.

Monin, A. S. and Obukhov, A. M.: Basic laws of turbulent mixing in the surface layer of the atmosphere, Contrib. Geophys. Inst. Acad. Sci. USSR, 24, 163–187, 1954.

Morrison, H. and Gettelman, A.: A New Two-Moment Bulk Stratiform Cloud Microphysics Scheme in the Community Atmosphere Model, Version 3 (CAM3). Part I: Description and Numerical Tests, Journal of Climate, 21, 3642 – 3659, https://doi.org/10.1175/2008JCLI2105.1, 2008.

Neale, R. B., Gettelman, A., Park, S., Chen, C.-C., Lauritzen, P. H., Williamson, D. L., Conley, A. J., Kinnison, D. E., Marsh, D., Smith, A. K., Vitt, F. M., García, R. R., Lamarque, J.-F., Mills, M. J., Tilmes, S., Morrison, H., Cameron-Smith, P., Collins, W. D., Iacono, M. J., Easter, M. C., Liu, X., Ghan, S. J., Rasch, P. J., and Taylor, M. A.: Description of the NCAR Community Atmosphere Model (CAM 5.0), Tech. rep., National Center for Atmospheric Research, https://doi.org/10.5065/wgtk-4g06, 2012.

Optis, M., Monahan, A., and Bosveld, F. C.: Limitations and breakdown of Monin–Obukhov similarity theory for wind profile extrapolation under stable stratification, Wind Energy, 19, 1053–1072, https://doi.org/10.1002/we.1883, 2016.

Ortega, J. M. and Rockoff, M. L.: Nonlinear difference equations and Gauss-Seidel type iterative methods, SIAM Journal on Numerical Analysis, 3, 497–513, 1966.

Rasch, P. J., Xie, S., Ma, P.-L., Lin, W., Wang, H., Tang, Q., Burrows, S. M., Caldwell, P., Zhang, K., Easter, R. C., Cameron-Smith, P., Singh, B., Wan, H., Golaz, J.-C., Harrop, B. E., Roesler, E., Bacmeister, J., Larson, V. E., Evans, K. J., Qian, Y., Taylor, M., Leung, L. R., Zhang, Y., Brent, L., Branstetter, M., Hannay, C., Mahajan, S., Mametjanov, A., Neale, R., Richter, J. H., Yoon, J.-H., Zender, C. S., Bader, D., Flanner, M., Foucar, J. G., Jacob, R., Keen, N., Klein, S. A., Liu, X., Salinger, A., Shrivastava, M., and Yang, Y.: An Overview of the Atmospheric Component of the Energy Exascale Earth System Model, Journal of Advances in Modeling Earth Systems, 11, 2377–2411, https://doi.org/10.1029/2019MS001629, 2019.

Reeves Eyre, J. E. J., Zeng, X., and Zhang, K.: Ocean Surface Flux Algorithm Effects on Earth System Model Energy and Water Cycles, Frontiers in Marine Science, 8, https://doi.org/10.3389/fmars.2021.642804, 2021.

Santos, S. P., Caldwell, P. M., and Bretherton, C. S.: Numerically Relevant Timescales in the MG2 Microphysics Model, Journal of Advances in Modeling Earth Systems, 12, e2019MS001 972, https://doi.org/10.1029/2019MS001972, e2019MS001972 10.1029/2019MS001972, 2020.

https://doi.org/10.5194/egusphere-2025-5430
Preprint. Discussion started: 21 January 2026

Vogl, C. J., Steyer, A., Reynolds, D. R., Ullrich, P. A., and Woodward, C. S.: Evaluation of Implicit-Explicit Additive Runge-Kutta Integrators for the HOMME-NH Dynamical Core, Journal of Advances in Modeling Earth Systems, 11, 4228–4244, https://doi.org/10.1029/2019MS001700, 2019.

Wan, H., Rasch, P. J., Taylor, M. A., and Jablonowski, C.: Short-term time step convergence in a climate model, Journal of Advances in Modeling Earth Systems, 7, 215–225, https://doi.org/10.1002/2014MS000368, 2015.

Wan, H., Zhang, S., Rasch, P. J., Larson, V. E., Zeng, X., and Yan, H.: Quantifying and attributing time step sensitivities in present-day climate simulations conducted with EAMv1, Geoscientific Model Development, 14, 1921–1948, https://doi.org/10.5194/gmd-14-1921-2021, 2021.

Wan, H., Zhang, K., Rasch, P. J., Larson, V. E., Zeng, X., Zhang, S., and Dixon, R.: CondiDiag1.0: a flexible online diagnostic tool for conditional sampling and budget analysis in the E3SM atmosphere model (EAM), Geoscientific Model Development, 15, 3205–3231, https://doi.org/10.5194/gmd-15-3205-2022, 2022.

Wan, H., Zhang, K., Vogl, C. J., Woodward, C. S., Easter, R. C., Rasch, P. J., Feng, Y., and Wang, H.: Numerical coupling of aerosol emissions, dry removal, and turbulent mixing in the E3SM Atmosphere Model version 1 (EAMv1) – Part 1: Dust budget analyses and the impacts of a revised coupling scheme, Geoscientific Model Development, 17, 1387–1407, https://doi.org/10.5194/gmd-17-1387-2024, 2024.

Xie, S., Lin, W., Rasch, P. J., Ma, P.-L., Neale, R., Larson, V. E., Qian, Y., Bogenschutz, P. A., Caldwell, P., Cameron-Smith, P., Golaz, J.-C., Mahajan, S., Singh, B., Tang, Q., Wang, H., Yoon, J.-H., Zhang, K., and Zhang, Y.: Understanding Cloud and Convective Characteristics in Version 1 of the E3SM Atmosphere Model, Journal of Advances in Modeling Earth Systems, 10, 2618–2644, https://doi.org/10.1029/2018MS001350, 2018.

Xie, S., Terai, C. R., Wang, H., Tang, Q., Fan, J., Burrows, S. M., Lin, W., Wu, M., Song, X., Zhang, Y., et al.: The Energy Exascale Earth System Model Version 3. Part I: Overview of the Atmospheric Component, Authorea Preprints, https://doi.org/https://doi.org/10.22541/essoar.174456922.21825772/v1, 2025.

Zeng, X., Zhao, M., and Dickinson, R. E.: Intercomparison of Bulk Aerodynamic Algorithms for the Computation of Sea Surface Fluxes Using TOGA COARE and TAO Data, Journal of Climate, 11, 2628 – 2644, https://doi.org/10.1175/1520-0442(1998)011<2628:IOBAAF>2.0.CO;2, 1998.

Zhang, S., Vogl, C. J., Larson, V. E., Bui, Q. M., Wan, H., Rasch, P. J., and Woodward, C. S.: Removing Numerical Pathologies in a Turbulence Parameterization Through Convergence Testing, Journal of Advances in Modeling Earth Systems, 15, e2023MS003633, https://doi.org/10.1029/2023MS003633, e2023MS003633 2023MS003633, 2023a.

Zhang, S., Vogl, C. J., Larson, V. E., Bui, Q. M., Wan, H., Rasch, P. J., and Woodward, C. S.: Removing Numerical Pathologies in a Turbulence Parameterization Through Convergence Testing, Journal of Advances in Modeling Earth Systems, 15, e2023MS003633, https://doi.org/10.1029/2023MS003633, 2023b.

Zwiers, F. W. and von Storch, H.: Taking Serial Correlation into Account in Tests of the Mean, Journal of Climate, 8, 336 – 351, https://doi.org/10.1175/1520-0442(1995)008<0336:TSCIAI>2.0.CO;2, 1995.